Journal of Hazardous Materials 435 (2022) 129029

Contents lists available at ScienceDirect

Journal of Hazardous Materials

journal homepage: www.elsevier.com/locate/jhazmat

Particulate matter and polycyclic aromatic hydrocarbon uptake in relation to leaf surface functional traits in Mediterranean evergreens: Potentials for air phytoremediation

Antonello Prigioniero [a], Daniela Zuzolo [a,*], Ülo Niinemets [b], Alessia Postiglione [a], Mariano Mercurio [a], Francesco Izzo [c], Marco Trifuoggi [d], Maria Toscanesi [d], Pierpaolo Scarano [a], Maria Tartaglia [a], Rosaria Sciarrillo [a], Carmine Guarino [a]

[a] Department of Science and Technology, University of Sannio, via de Sanctis snc, Benevento 82100, Italy
[b] Institute of Agricultural and Environmental Sciences, Estonian University of Life Sciences, Fr. R. Kreutzwaldi 1, Tartu 51006, Estonia
[c] Department of Earth Sciences, Environment and Resources, University of Naples Federico II, via Cintia, Naples 80126, Italy
[d] Department of Chemical Sciences, University of Naples Federico II, via Cintia, Naples 80126, Italy

HIGHLIGHTS

- Leaf surface functional traits of Mediterranean evergreen species were analysed.
- PM and PAHs concentrations in leaves were observed in a 30-day study in Naples.
- Functional traits were related to the leaves capacity for uptake air pollutants.
- Trichomes have a greater influence on the uptake of heavy and coarse pollutants.
- Lighter PAHs uptake is also regulated by the chemical properties of the cuticle.

GRAPHICAL ABSTRACT

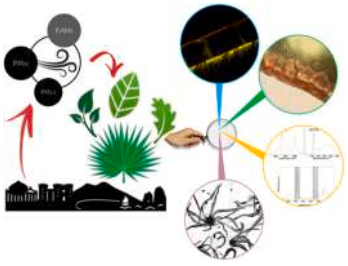

ARTICLE INFO

Editor: Dr. Guillaume Echevarria

Keywords:
Plant functional traits
Air phytoremediation
Air pollution
Particulate matter
Polycyclic aromatic hydrocarbons

ABSTRACT

We explored relationships between particulate matter (PM) and polycyclic aromatic hydrocarbon (PAHs) leaf concentrations, uptake rates and leaf surface functional traits in four Mediterranean evergreen trees (*Chamaerops humilis*, *Citrus* × *aurantium*, *Magnolia grandiflora*, and *Quercus ilex*) during a dry month. Pollutant leaf concentration at different dates and uptake rate were correlated. We quantified PM by gravimetric analysis, PAHs were extracted from intact and dewaxed leaves and analyzed by GC-MS, and cuticle thickness, number and surface of stomata (N_s and S_S) and trichomes (N_t and S_t) were determined by optical microscopy. Infrared spectroscopy was used to investigate the leaves surfaces composition and assess esterification index (E). Studied species were characterized by unique combinations of functional traits and pollutant uptake capacities. PM_{10} uptake scaled positively with S_S, S_t and upper cuticle thickness ($T_{c,u}$) across species. $PM_{2.5}$ uptake scaled positively with $T_{c,u}$, and thicker cuticles were also associated with greater shares of uptake of hydrophobic PM fractions. Uptakes of different fractions of PAH were generally weakly related to different leaf functional traits, except for some correlations with E and S_S. We conclude that both plant surface morphological and chemical leaf traits influence PM and PAH retention, unveiling their potential role in air phytoremediation.

* Corresponding author.
E-mail address: dzuzolo@unisannio.it (D. Zuzolo).

https://doi.org/10.1016/j.jhazmat.2022.129029
Received 19 January 2022; Received in revised form 22 April 2022; Accepted 25 April 2022
Available online 29 April 2022

1. Introduction

Air pollution belongs to environmental hazards with serious adverse consequences for human health (Costabile et al., 2020; Fusaro et al., 2021). Among different airborne pollutants, particulate matter (PM), including coarse (PM_{10}), fine ($PM_{2.5}$) and ultra-fine ($PM_{0.2}$) components, is most dangerous due to causing chronic health problems such as cardio-respiratory diseases and diabetes (Horemans et al., 2012; Zhang et al., 2019). Furthermore, airborne particulate matter binds polycyclic aromatic hydrocarbons (PAHs) and potentially toxic elements (PTEs), further enhancing their adverse impacts on health (Chen et al., 2021; Fellet et al., 2016; Fusaro et al., 2021; Grote et al., 2016; Jouraeva et al., 2003; Li et al., 2021). Sixteen PAHs, distinguished in three classes based on molecular mass (high molecular mass - HMM; medium molecular mass - MMM; low molecular mass - LMM), have been identified as a priority for air pollution studies (Thiombane et al., 2019) and have become targets of environmental studies in many countries (Fellet et al., 2016; Peng et al., 2012).

Urban forests contribute to human health and well-being through a multitude of ecosystem services, even by mitigating PM and PAHs impacts and ameliorating air quality through four processes, absorption, dry particle deposition, rain dissolution and wet particle deposition (Baraldi et al., 2019; Chiam et al., 2019; Grote et al., 2016; Nowak et al., 2013; Howsam et al., 2001; Gong et al., 2021). Studies have demonstrated a large interspecific variability in the capacity to sequester and retain PM and PAHs in leaves (Dzierzanowski et al., 2011; Li et al., 2019; Mo et al., 2015; Mori et al., 2015; Pace and Grote, 2020; Sæbø et al., 2012). However, due to study-to-study differences in experimental and environmental conditions, estimates of species phytoremediation capacities are not directly comparable among studies (Chiam et al., 2019; Prigioniero et al., 2021).

Plant contribution to atmospheric pollution mitigation depends on complex interactions between biotic and abiotic environmental factors, pollutant concentrations and functional traits (Baraldi et al., 2019; Esposito et al., 2020; Fellet et al., 2016; Grote et al., 2016; Tian et al., 2019). Leaves are the main actors in providing these services and the leaf structural features influence plants efficiency in PM removal from urban atmosphere (Liu et al., 2012). Leaf surface characteristics including cuticular properties, presence and density of glandular and non-glandular trichomes, stomatal size and number, leaf internal structure and physiological activity are the key functional traits that can alter the performance of species in air phytoremediation (Esposito et al., 2020; Zhang et al., 2017; Li et al., 2018; Niinemets et al., 2014). Leaf surface chemical and physical characteristics, in particular, its hydrophobicity, effective surface area and effective porosity as determined by presence of protruding epicuticular waxes and trichomes, play a major role in uptake of large slowly diffusing pollutants such as PM and PAHs (Baraldi et al., 2019; Chiam et al., 2019; Fellet et al., 2016; Grote et al., 2016). The cuticle chemical composition and physical structure strongly vary among plant species and influence the interfacing between the underlying tissues and the external environment, as well as performance in air phytoremediation (Buda et al., 2009; Domínguez et al., 2015; Heredia-Guerrero et al., 2016; Riederer and Müller, 2006). The role of the cuticle in remediation of PM and PAHs has been postulated to depend mainly on its hydrophobicity, but cuticles also strongly differ in thickness and effective porosity (Jouraeva et al., 2003; Li et al., 2017). Stomata are the sites for pollutant entry into leaf interior, and the functional traits included in air phytoremediation studies are number and size (Chen et al., 2017; Baraldi et al., 2019), arrangement (Sæbø et al., 2012; Baraldi et al., 2019; Chiam et al., 2019), and shape (Chen et al., 2017). Trichomes enhance surface complexity and determine sites for pollutants entrapment and absorption, and functional traits used to characterize pollutant removal from ambient air are trichome size (Grote et al., 2016) and density (Baraldi et al., 2019; Chiam et al., 2019; Fellet et al., 2016). Yet, there is little information of integrated functional traits such as stomatal pore area per leaf area and trichome area per leaf area that could be more quantitatively linked to pollutant uptake than size, number and shape. Furthermore, few studies have simultaneously looked at the whole suites of traits that could alter the uptake of different classes of pollutants, and the relationships between the functional traits and plant species performance in removal of air pollutants were often inconsistent (Corada et al., 2021).

In this study, we aimed to explore the relationships of leaf concentrations and daily uptake rate of PM and PAHs with leaf surface functional traits (Table 1) in wide-spread Mediterranean species with contrasting leaf characteristics. We hypothesized that absorption of different pollutants scales positively with trichome surface area, absorption and cuticular uptake of more hydrophobic pollutants with surface hydrophobicity and cuticle thickness. Furthermore, we hypothesized that the uptake and concentration of smaller molecular mass compounds and smaller particles are mostly influenced by stomata-related traits. To test these hypotheses, we estimated the stomatal and trichome surface areas and numbers per leaf area, the degree of cuticle esterification, and cuticle thickness. A double sampling campaign was carried out in the city center of Naples (Southern Italy) to investigate the capacity of plant species to accumulate air pollutants (PM_{10}, $PM_{2.5}$ and PAHs) from urban air by leaves of four most abundant evergreen tree species in the area: *Chamaerops humilis* L. (Mediterranean dwarf palm), *Citrus* × *aurantium* L. (bitter orange), *Magnolia grandiflora* L. (southern magnolia), and *Quercus ilex* L. (holm oak). Our results demonstrate important general relationships among pollutant uptake and leaf functional traits, but also highlight a large species-specific component that also contributes to species variation in uptake of major pollutants from ambient air.

2. Methods

2.1. Site description and sample collection

The study was conducted in the urban area of Naples, Southern Italy (40°50′ N 14°15′ E, 17 m above sea level) from the 1st of August 2019 (D_0) to the 1st of September 2019 (D_1). The city of Naples is affected by a growing urban heat island effect as well as by frequent periods of high pollution levels due to the topographical features of the region and considerable anthropogenic emission sources (Fortelli et al., 2016). The climate is Mediterranean, Köppen subtype Csa (hot summer Mediterranean climate; Kottek et al., 2006), with average annual rainfall of 1080 mm and average annual temperature of 16.5 °C ("Climate Data, 2021). Public squares and major avenues within the core of Naples urban area were selected based on the following two criteria: (1) the locations selected were in or next to the major traffic corridors, and (2) the locations were as close as possible to the meteorological and air quality monitoring stations of the Campania Regional Environmental Protection Agency (ARPAC) network (Fellet et al., 2016; Fig. 1). Two sampling sites were identified for each of the four selected species (*C. humilis*, *C.* × *aurantium*, *M. grandiflora*, and *Q. ilex*). In each sampling site, depending on tree availability, seven to ten trees per species were chosen and georeferenced with a GPS (Table S1 in Supplementary File). From each tree, 5–15 leaves were randomly collected from 5 to 10 branches per tree. Only branches facing the road at a maximum height of 2 m from the ground were sampled to maximize the pollution impact. All the sampled leaves for given species at each sampling site were pooled, and stored in plastic bags prior to analyses (at most for 48 h). A limitation of this work is that we were unable to find data on air concentrations of polycyclic aromatic hydrocarbons for the period between D_0 and D_1.

2.2. Characterization of leaf functional traits

2.2.1. Number of stomata and stomatal surface per leaf area

Stomatal number per surface area for upper ($N_{s,u}$) and for lower ($N_{s,l}$) leaf surface were assessed as in Kardel et al. (2010). Three leaves of each

Table 1 –
List of abbreviations used.

	Symbol	Unit of measure	Description
	$N_{s,u}$	m^{-2}	Number of stomata per unit upper surface area
	$N_{s,l}$	m^{-2}	Number of stomata per unit lower surface area
	$N_{t,l}$	m^{-2}	Number of trichomes per unit lower surface area
	$T_{c,u}$	μm	Cuticle thickness, upper surface
	$T_{c,l}$	μm	Cuticle thickness, lower surface
	S_s	$m^2\ m^{-2}$	Surface of stomata per leaf unit surface area
	S_{sp}	$m^2\ m^{-2}$	Surface of stomata pore per leaf unit surface area
	S_t	$m^2\ m^{-2}$	Surface of trichome per leaf unit surface area
Leaf Surface Functional Traits	E_u		Esterification index, upper surface
	E_l		Esterification index, lower surface
	D_0	d	Date of first sampling
	D_1	d	Date of second sampling
Experimental Setup	Δt	D	Period between the two samplings and exposure period
	$C_{PM2.5,a}$	$\mu g\ m^{-3}$	Mean daily air concentration of $PM_{2.5}$
Environmental conditions	$C_{PM10,a}$	$\mu g\ m^{-3}$	Mean daily air concentration of PM_{10}
	$C_{PM2.5,D0}$	$\mu g\ m^{-2}$	Concentration of $PM_{2.5}$ taken up by the leaf at D_0
	$C_{PM2.5,D1}$	$\mu g\ m^{-2}$	Concentration of $PM_{2.5}$ taken up by the leaf at D_1
	$\Theta_{PM2.5}$		Ratio between the $PM_{2.5}$ extracted with chloroform and $PM_{2.5}$ total extracted
	$C_{PM10,D0}$	$\mu g\ m^{-2}$	Concentration of PM_{10} taken up by the leaf at D_0
	$C_{PM10,D1}$	$\mu g\ m^{-2}$	Concentration of PM_{10} taken up by the leaf at D_1
	Θ_{PM10}		Ratio between the PM_{10} extracted with chloroform and PM_{10} total extracted
	$C_{LMM,D0,i}$	$\mu g\ m^{-2}$	Concentration of low molecular mass compounds taken up by the intact leaf D_0
	$C_{LMM,D1,i}$	$\mu g\ m^{-2}$	Concentration of low molecular mass compounds taken up by the intact leaf at D_1
	$C_{LMM,D0,dw}$	$\mu g\ m^{-2}$	Concentration of low molecular mass compounds taken up by the dewaxed leaf D_0
	$C_{LMM,D1,dw}$	$\mu g\ m^{-2}$	Concentration of low molecular mass compounds taken up by the dewaxed leaf at D_1
	$C_{MMM,D0,i}$	$\mu g\ m^{-2}$	Concentration of medium molecular mass compounds taken up by the intact leaf D_0
	$C_{MMM,D1,i}$	$\mu g\ m^{-2}$	Concentration of medium molecular mass compounds taken up by the intact leaf at D_1
	$C_{MMM,D0,dw}$	$\mu g\ m^{-2}$	Concentration of medium molecular mass compounds taken up by the dewaxed leaf D_0
	$C_{MMM,D1,dw}$	$\mu g\ m^{-2}$	Concentration of medium molecular mass compounds taken up by the dewaxed leaf at D_1
	$C_{HMM,D0,i}$	$\mu g\ m^{-2}$	Concentration of high molecular mass compounds taken up by the intact leaf D_0
	$C_{HMM,D1,i}$	$\mu g\ m^{-2}$	Concentration of high molecular mass compounds taken up by the intact leaf at D_1
	$C_{HMM,D0,dw}$	$\mu g\ m^{-2}$	Concentration of high molecular mass compounds taken up by the dewaxed leaf D_0
Pollutants concentrations	$C_{HMM,D1,dw}$	$\mu g\ m^{-2}$	Concentration of high molecular mass compounds taken up by the dewaxed leaf at D_1
	C_{PM10}	$\mu g\ m^{-2}$	Mean leaf concentration of PM_{10} for the two measurement dates, D_1 and D_0
	$C_{PM2.5}$	$\mu g\ m^{-2}$	Mean leaf concentration of $PM_{2.5}$ for the two measurement dates, D_1 and D_0
	$C_{LMM,i}$	$\mu g\ m^{-2}$	Mean intact leaf concentration of LMM for the two measurement dates, D_1 and D_0
	$C_{MMM,i}$	$\mu g\ m^{-2}$	Mean intact leaf concentration of MMM for the two measurement dates, D_1 and D_0
	$C_{HMM,i}$	$\mu g\ m^{-2}$	Mean intact leaf concentration of HMM for the two measurement dates, D_1 and D_0
	$C_{LMM,dw}$	$\mu g\ m^{-2}$	Mean dewaxed leaf concentration of LMM for the two measurement dates, D_1 and D_0
	$C_{MMM,dw}$	$\mu g\ m^{-2}$	Mean dewaxed leaf concentration of MMM for the two measurement dates, D_1 and D_0
	$C_{HMM,dw}$	$\mu g\ m^{-2}$	Mean dewaxed leaf concentration of HMM for the two measurement dates, D_1 and D_0
	U_{PM10}	$\mu g\ m^{-2}\ d^{-1}$	daily uptake rate of PM_{10}
	$U_{PM2.5}$	$\mu g\ m^{-2}\ d^{-1}$	daily uptake rate of $PM_{2.5}$
	$U_{LMM,i}$	$\mu g\ m^{-2}\ d^{-1}$	daily uptake rate of low molecular mass compounds for intact leaf
	$U_{LMM,dw}$	$\mu g\ m^{-2}\ d^{-1}$	daily uptake rate of low molecular mass compounds for dewaxed leaf
	$U_{MMM,i}$	$\mu g\ m^{-2}\ d^{-1}$	daily uptake rate of medium molecular mass compounds for intact leaf
	$U_{MMM,dw}$	$\mu g\ m^{-2}\ d^{-1}$	daily uptake rate of medium molecular mass compounds for dewaxed leaf
	$U_{HMM,i}$	$\mu g\ m^{-2}\ d^{-1}$	daily uptake rate of high molecular mass compounds for intact leaf
Uptake rate	$U_{HMM,dw}$	$\mu g\ m^{-2}\ d^{-1}$	daily uptake rate of high molecular mass compounds for dewaxed leaf

species were randomly selected and a stomatal imprint was made using a thin coat of colorless nail varnish on both sides of the leaf, avoiding midrib and leaf margins. Because the leaves of *Q. ilex*, *M. grandiflora* and *C. humilis* have a dense layer of trichomes on the lower side, the nail varnish was applied twice on the lower surface. Upon the first application, the trichomes were removed with the nail varnish. The stomatal imprint was obtained after second application of nail varnish. A transparent cellulose adhesive tape was sticked onto the dried nail varnish, and gently peeled off and attached to a glass slide. Stomatal imprints were viewed under a light microscope (Nikon Eclipse E600) at 600x magnification, and digital images were taken with Motic Image Plus 3.0 software (Fig. 2). Five random points (1 mm^2) were selected for stomatal observations in each leaf. The number of stomata per surface area was counted from each field of view. In each field of view, five stomata were randomly selected, and the length and width of individual stomatal pores (l_{sp} and w_{sp}) and stomatal guard cells (l_s and w_s) were measured and averaged, and areas of stomatal pores and stomata were estimated by approximating their shape by ellipses. Ultimately, the fraction of stomatal area in total leaf area (S_s, $m^2\ m^{-2}$) and the fraction of stomatal pore area in total leaf area (S_{sp}, $m^2\ m^{-2}$) were estimated as:

$$S_s = (\overline{l_s}/2)(\overline{w_s}/2)\pi N_s \quad (1)$$

$$S_{sp} = (\overline{l_{sp}}/2)(\overline{w_{sp}}/2)\pi N_s, \quad (2)$$

where $\overline{l_s}$ is the average stomatal length (m), $\overline{w_s}$ the average stomatal width (m), $\overline{l_{sp}}$ the average stomatal pore length (m), $\overline{w_{sp}}$ the average stomatal pore width (m) and N_s the number of stomata per leaf area (m^{-2}).

2.2.2. Cuticle thickness

Three randomly selected leaves of each species were fixed in FAA fixative (10% formaldehyde; 5% acetic acid; 50% ethanol; 35% deionized water) immediately after excision. Freehand sections of each leaf were obtained and stained with fat-soluble Sudan IV stain as described by (Buda et al., 2009) to visualize the cuticle and measure its thickness. Sudan IV stock solution (0.1% w / v in isopropyl alcohol) was diluted in 3:2 ratio with distilled water. The red stain was added to the freehand sections for 30 min and then rinsed first with 50% isopropyl alcohol and then with distilled water. Slides were mounted in distilled water with a cover slip and viewed with a Nikon Eclipse E600 light microscope with epifluorescence in bright field at 1000x magnification, and the thickness of upper cuticle ($T_{c,u}$) and lower ($T_{c,l}$) cuticle were measured (Fig. 1 for representative leaf images). When the lower cuticle was not discernible, $T_{c,l}$ could not be measured. Five random spots in the sections were selected and measured for cuticle thickness.

2.2.3. Non-glandular trichome number, surface per leaf area and morphology

Due to extremely dense trichome mat on the leaf underside of some species, the trichomes were first removed with nail varnish as explained above for estimation of stomatal number. After removing the bulk of trichomes, the nail varnish was applied again to obtain the surface imprints. The imprints were peeled off with a cellulose adhesive tape, attached to a microscope slide and viewed at 200x magnification with a Nikon Eclipse E600 light microscope, and digital images were taken using Motic Image Plus 3.0 software. The trichome bases remaining after trichome removal were counted from digital images to estimate the number of trichomes per unit leaf area (N_t, m^{-2}). Three leaves of each species were randomly selected and for each leaf, trichomes were counted in five random locations of 1 mm^2.

To characterize trichome morphology and estimate trichome surface per leaf area, S_t (m^2 m^{-2}), trichomes removed with the adhesive tape were viewed under the light microscope at 200x magnification. Depending on the morphology detected, trichome shapes were approximated by simple geometric solids (cylinders or cones) and the S_t was calculated. For the conical shape, S_t was calculated from trichome width (w_t, m) and length (l_t, m) as:

$$S_t = \pi \frac{\overline{w_t}}{2} \sqrt{\left(\frac{\overline{w_t}}{2}\right)^2 + \overline{l_t}^2} N_t \quad (3)$$

For each leaf, three trichomes, randomly chosen from five random leaf positions, were selected and measured, and the average width ($\overline{w_t}$, m) and length ($\overline{l_t}$, m) were calculated. *Quercus ilex* had stellate trichomes, and their surface area per leaf area (S_t, m^2 m^{-2}) was measured considering the base of trichome as a cylinder and the branches as cones. The lateral surfaces of these shapes were calculated using the trichome base width (w_{tb}, m) and length (l_{tb}, m), the branch width (w_t, m) and

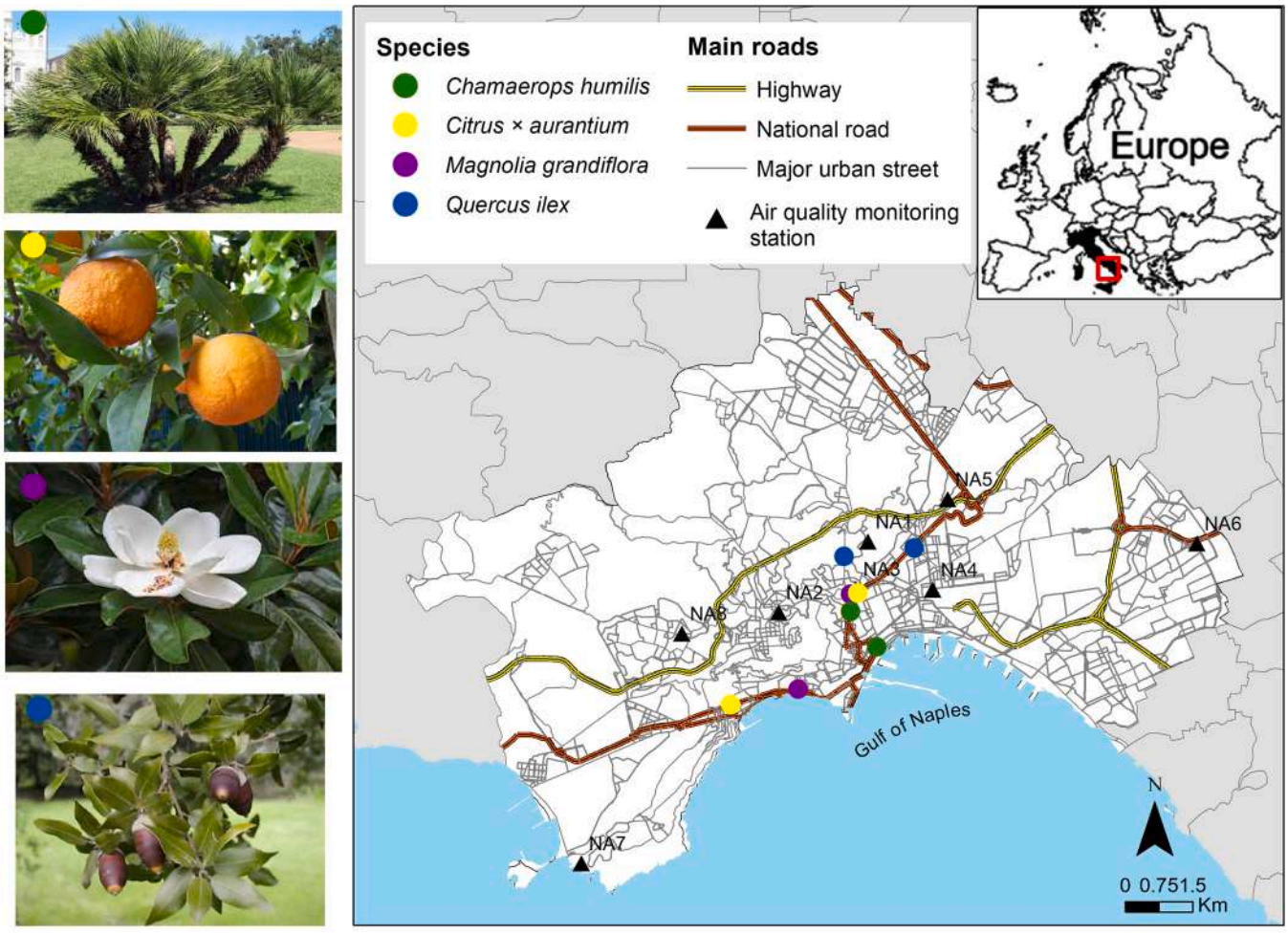

Fig. 1. – Sampled plant species, and the study area with sampling points, air quality monitoring stations, and road network (Naples city, Southern Italy 40°50′ N 14°15′ E).

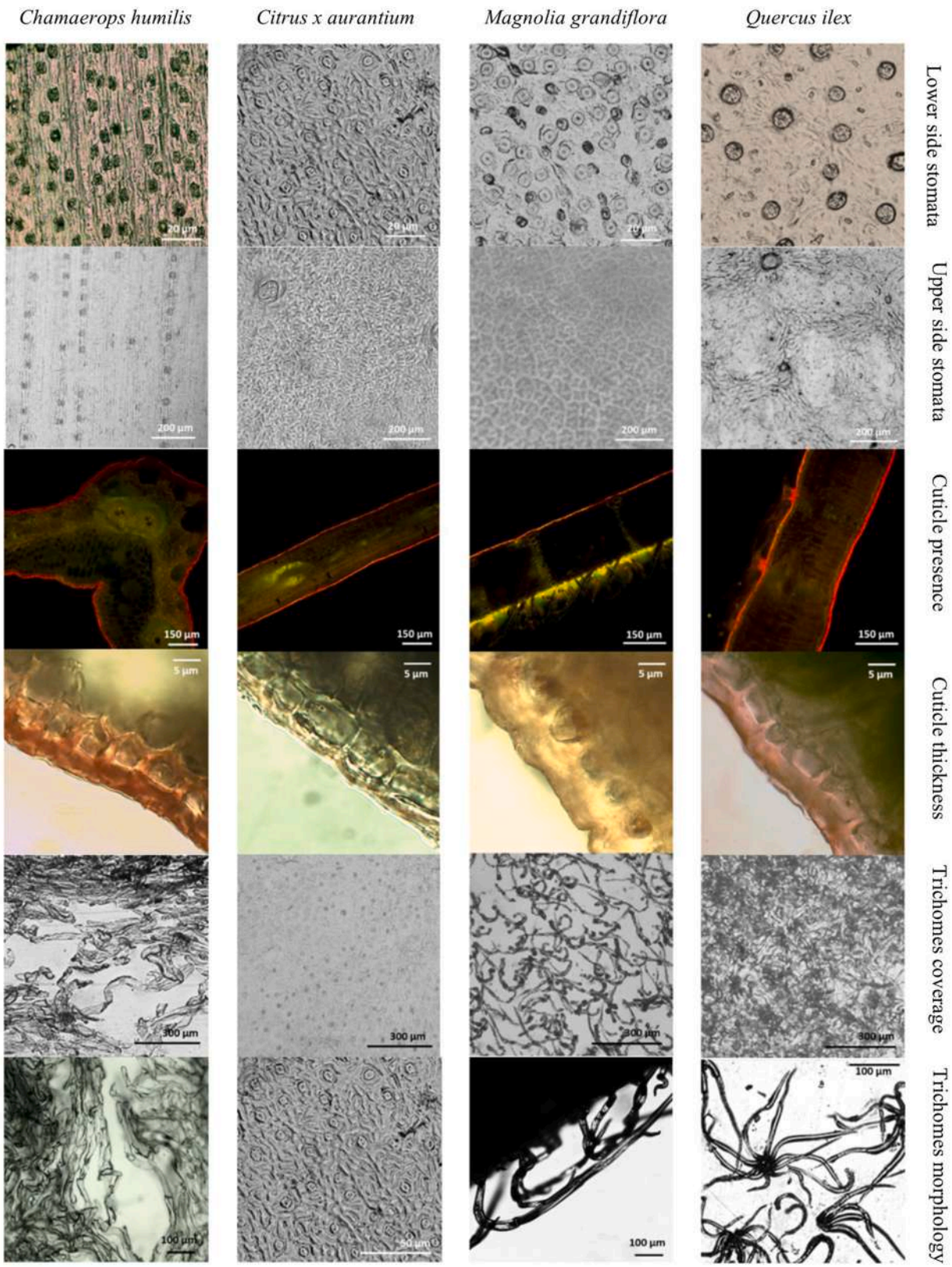

Fig. 2. – Representative microscopy images used for determination of leaf surface functional traits in the four studied species. The samples were viewed in bright field and epifluorescence using a Nikon Eclipse E600 light microscope at magnifications ranging from 600x-1000x. Digital images were taken with Motic Image Plus 3.0 software. From the images, number of stomata on lower and upper leaf surface ($N_{s,l}$ and $N_{s,u}$), number of trichomes (N_t), cuticle thickness of lower and upper leaf side ($T_{c,l}$ and $T_{c,u}$), and stomatal surface area per leaf area (S_s) and stomatal pore area per leaf area (S_{sp}) and trichome area per leaf area (S_t) were estimated. The presence of the cuticular layer (fluorescent in red) is clearly visible in the upper and lower side of the leaves in *C. humilis*, *C.* × *aurantium* and *Q. ilex*. The cuticle in the lower side of *M. grandiflora* leaves was not clearly discernible with the methodology used.

length (l_t, m), and the number of branches (n):

$$S_t = \pi\overline{w_{tb}}\overline{l_{tb}} + \overline{n}\left(\pi\frac{\overline{w_t}}{2}\sqrt{\left(\frac{\overline{w_t}}{2}\right)^2 + \overline{l_t}^2}\right)N_t \quad (4)$$

For each leaf, three trichomes, randomly chosen from five random spots, were measured, and the averaged value of trichome base width ($\overline{w_{tb}}$, m) and length ($\overline{l_{tb}}$, m), branch width ($\overline{w_t}$, m) and length ($\overline{l_t}$, m), and number of branches ($\overline{n}$) were calculated for each spot.

2.2.4. Fourier-transform infrared spectroscopy (FTIR) analyses of leaf surface

Leaf surface chemical characteristics were analyzed with a FTIR spectrometer (Bruker Alpha) using the attenuated total reflectance (FTIR-ATR) mode (spectral range 4000–400 cm^{-1}, resolution 4 cm^{-1}, 128 scans). The beam penetration depth (Equation S1 in Supplementary Information) generally ranged from 0.5 μm to 5 μm, and thus, most of the spectral features observed in the selected leaves (Fig. 3 and Table S3 in Supplementary Information) should be attributable to the stretching and bending vibrations of cuticle in upper leaf side, and of cuticle and trichomes when they are present in lower leaf side.

The obtained spectra were baseline corrected, and the esterification index (Heredia-Guerrero et al., 2016, Fig. S1) was calculated for lower and upper leaf sides (Heredia-Guerrero et al., 2016). Esterification index characterizes the degree of cross-linkage of cutin-forming hydroxy- and peroxyacids (Heredia-Guerrero et al., 2016). Esterification index is greater for the cutin with a degree of cross-linkage of fatty acids. Cutin cross-linking is a useful characteristic to make qualitative comparisons between species and to derive information on the presence of polymeric (non-extractable) lipids in the leaf surface matrix, which represent the most effective barrier to the movement of polycyclic aromatic hydrocarbons from the environment to the inner leaf tissues (Heredia-Guerrero et al., 2016; Li et al., 2017). The esterification index (E) has been obtained from the ratio between the absorbance intensity (A) of the stretching vibration ν(C═O) of esters at 1730 cm^{-1} and the asymmetric stretching vibration $\nu_a(CH_2)$ of methylene at 2916 cm^{-1} as:

$$E = A_{\nu(C=O)}/A_{\nu_a(CH_2)} \quad (5)$$

The index was estimated for both lower (E_l) and upper (E_u) leaf surfaces. Five random leaves were selected from the pooled leaf samples and used for FTIR analyses. The spectra were processed with the software Opus 7.2 (Bruker, Optics GmbH).

2.3. Particulate matter concentrations

For each species, two subsamples were taken from each sampling location, consisting of a variable number of randomly selected leaves (due to different shapes and sizes of leaves of different species). The amount of leaf area in each subsample was about 0.07 m^2. These leaves were used to quantify the concentrations of fine and coarse particulate matter at different sampling dates, in the beginning ($C_{PM2.5,\ D0}$, $C_{PM10,\ D0}$) and at the end ($C_{PM2.5,\ D1}$, and $C_{PM10,\ D1}$) of the study (Table 1). PM_{10} and $PM_{2.5}$ were extracted from the leaves according to Dzierzanowski et al. (2011). The extraction protocol involves an initial washing of the plant material with distilled water to remove particulate matter deposited on the surface. The solution resulting from the washing of the selected leaves was sieved using a metal sieve with mesh diameter 100 μm to eliminate particles larger than 100 μm, then it was vacuum-filtered using pre-weighted, stabilized filters with different porosity to retain PM_{10} (filter paper grade 91, Whatman™) and $PM_{2.5}$ (filter paper grade 42, Whatman™). After filtration, the filters were dried and weighed, and the difference in mass was recorded. The operation was repeated with the same leaves, using chloroform ($CHCl_3$) instead of distilled water to extract the epicuticular waxes and related particulate matter. The contents of $PM_{2.5}$ and PM_{10} were expressed per unit leaf surface area. The resulting dewaxed leaves were used for subsequent chemical analysis of polycyclic aromatic hydrocarbons (PAHs) together with subsamples of intact leaves (which did not undergo any treatment). The concentrations of coarse and fine particulate matter extracted with chloroform were divided by the total extracted coarse and fine particulate matter to derive indices characterizing the influence of the hydrophobic component on the accumulation capacity of coarse and fine particulate matter (Θ_{PM10} and $\Theta_{PM2.5}$) in the investigated species (Dzierzanowski et al., 2011; Popek et al., 2013).

2.4. PAH concentrations

To quantify the concentrations of low, medium and high molecular mass PAH in intact leaves at the first sampling date ($C_{LMM,D0,i}$, $C_{MMM,D0,i}$, $C_{HMM,D0,i}$), in intact leaves at the second sampling date ($C_{LMM,D1,i}$, $C_{MMM,D1,i}$, $C_{HMM,D1,i}$), in dewaxed leaves at the first sampling date ($C_{LMM,D0,dw}$, $C_{MMM,D0,dw}$, $C_{HMM,D0,dw}$), and in dewaxed leaves at the second sampling date ($C_{LMM,D1,dw}$, $C_{MMM,D1,dw}$, $C_{HMM,D1,dw}$) (Table 1), the samples of intact leaves, and dewaxed leaves were dried at room temperature for 48–72 h. About 2.0 g of dry sample was extracted with 20 ml acetone-hexane mixture (1:1 v/v) using an ultrasonic extractor for 10 min (Sonica, SOLTEC, Italy). The extract was concentrated with an evaporator under nitrogen flow to a final volume of 1 ml (Multivap10, Labtech, Italy). The extract was cleaned on a sulphate sodium anhydrous column and, then 10 μL of the internal standard was added (mixture of 5 deuterated PAHs at the concentration of 10 mg L^{-1}) and injected into a gas chromatograph (GCMS-TQ8030 Shimadzu, Japan) coupled with a triple quadrupole mass spectrometer (MS-TQ8030, Shimadzu, Japan) and a fused silica HP5-MS capillary column (30 m length × 0.25 mm inner diameter, film thickness 0.25 μm; Agilent Technologies, US). The separation was conducted with oven temperature programmed as follows: initial setting at 80 °C (2 min hold) ramped to 180 °C at 20 °C min^{-1} and finally to 300 °C at 5 °C min^{-1} (9 min hold). The injector was held at 280 °C. The mass spectrometer was operated in SIM (selected ion monitoring) mode. The selected ions are reported in Table 2. The identification of PAHs in the solutions extracted was carried out based on previously determined retention times, and it was confirmed using mass spectra of the NIST library (NIST 20, 2020). The quantification of PAHs was performed using an external calibration curve together with the internal standards. The detection limit (LOD) and limit of quantification (LOQ) for each investigated PAH were calculated using the range method of prediction to 95% of linear regressions. The calculated averages of LOD and LOQ in the matrix of leaf were 0.007 μg m^{-2} and 0.02 μg m^{-2}. The data quality is ensured by certified reference materials (CRM-NIST 3253) and the recovery percentage was estimated by analyzing in triplicate the CRM and the observed range was 70–110%.

2.5. Estimation of pollutant uptake rate (R)

We used meteorological data and ambient air PM_{10} and $PM_{2.5}$ concentrations measured at 8 stations (Fig. 1) distributed in the urban area of Naples (30 days, Δt, from D_0 to D_1; daily bulletins of ARPAC, www.arpacampania.it). The wind direction information was considered as directional components in the prediction of pollutants spatial distribution. Hence, monthly average spatial distribution of PM_{10} and $PM_{2.5}$ was modelled (data not shown) to assess the mean daily concentration of fine and coarse particulate matter in the air next to the foliage of sample plant specimens ($C_{PM2.5,\ a}$ and $C_{PM10,\ a}$, μg m^{-3}). The data were averaged to obtain concentrations of fine and coarse particulate matter in the air ($C_{PM2.5,a}$ and $C_{PM10,a}$) (Table 1), also considering the dominant wind direction. The uptake rate (U) was estimated for each pollutant as:

$$U = \frac{(C_{D1} - C_{D0})}{\Delta t} \quad (6)$$

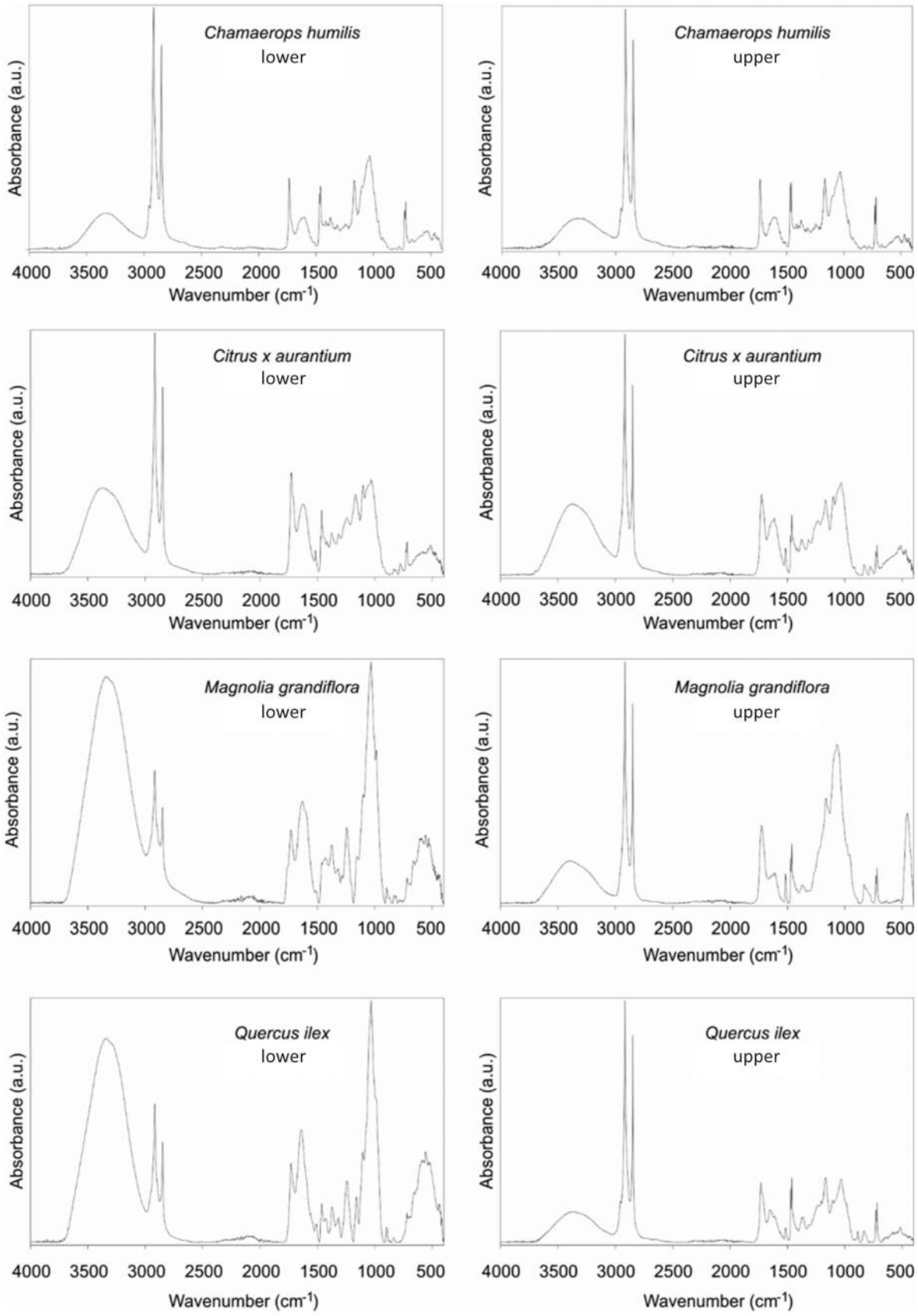

Fig. 3. – *Chamaerops humilis*, *Citrus* × *aurantium*, *Magnolia grandiflora* and *Quercus ilex* (ATR-FTIR) spectra of lower and upper leaf surfaces.

Table 2
List of groups of polycyclic aromatic hydrocarbons (PAHs) analyzed, the deuterated standards employed (underlined), the quantification ions and confirmation ions for SIM mode in the GC-MS analysis.

PAHs congener	Quantification Ion	Confirmation Ions	PAHs Category
Naphthalene	128	64, 127	
Acenaphthylene	152	76, 151	
Naphthalene D8 (IS)	136	–	
Acenaphthene	154	76, 152	
Fluorene	166	82, 165	LMM
Acenaphthene D10 (IS)	164	–	
Anthracene	178	89, 188	
Phenanthrene	178	89, 188	
Fluoranthene	202	101, 200	
Pyrene	202	101, 200	
Tetraphene	228	114, 226	
Phenanthrene D10 (IS)	188	–	
Chrysene	228	114, 226	MMM
Benzo(b)fluoranthene	252	126, 250	
Benzo[k]fluoranthene	252	126, 250	
Benzo[e]pyrene	252	126, 250	
Benzo[a]pyrene	252	126, 250	
Chrysene D12 (IS)	240	–	
Indeno[1,2,3-cd] pyrene	276	138, 277	
Dibenz[a,h] anthracene	278	139, 279	
Benzo[ghi]perylene	276	138, 277	
Perylene D12 (IS)	264	–	HMM

PAHs are grouped in three categories by molecular mass: low molecular mass (LMM), medium molecular mass (MMM), and high molecular mass (HMM).

2.6. Data analyses

Prior to statistical analyses, data were log transformed to normalize the distributions and residuals (Mahapoonyanont et al., 2010). Statistical analyses were performed in R environment (R Core Team, 2015). Analysis of variance (ANOVA) followed by Tukey's Honest Significant Difference (Tukey's HSD) post-hoc test was used to test for species differences in *U* and *C*. In the second step, one-way multivariate analysis of variance (one-way MANOVA) using Pillai's trace criterion was used to test for species differences in leaf functional traits. Pollutant concentration and uptake values were correlated with the functional traits of the leaves surfaces to test for the relationships between the rates of accumulation of PM as well as PAHs and the characteristics of trichomes, cuticle and stomata. R package *corrplot* (Wei and Simko, 2021) was used as a visual exploratory tool to analyze the correlations among leaf functional traits and contaminant accumulation. Finally, a two-dimensional PCA biplot was generated to distinguish and depict the main patterns in the dataset (Wickham, 2016). All statistical tests were considered significant at $p < 0.05$.

3. Results

3.1. Leaf surface functional traits

Number of stomata on the lower leaf side ($N_{s,l}$) varied from 2.22 10^8 m^{-2}-3.91 10^8 m^{-2} among the species (Table 3). *Quercus ilex* had almost two-fold greater $N_{s,l}$ than the other species (Table 3). *Chamaerops humilis* was the only amphistomatous species with stomata on both leaf sides (Table 3; Fig. 2). The surface area of stomata per leaf area (S_s) and surface area of stomatal pores per leaf area (S_{sp}) varied from 0.0542 m^2 m^{-2} to 0.1461 m^2 m^{-2} and from 0.0084 m^2 m^{-2} to 0.0204 m^2 m^{-2} (Table 3). Although *Q. ilex* had the highest stomatal surface area per leaf area, *C. humilis* had the highest stomatal pore surface per leaf area, followed by *Q. ilex*, *M. grandiflora* and *C.* × *aurantium* (Table 3).

Cuticle thickness of the lower leaf side ($T_{c,l}$) varied from 3.63 μm to 5.37 μm (Table 3). *Chamaerops humilis* and *Q. ilex* leaves showed the thickest lower cuticle thickness, followed by *C.* × *aurantium* (Table 3). With the methodology used in this work, it was not possible to determine the thickness of the lower cuticle of *M. grandiflora* leaves (Table 3).

Thickness of cuticle of the upper leaf side ($T_{c,u}$) separated the species among two groups: the first group included *C.* × *aurantium* (5.0 μm) and *C. humilis* (6.6 μm) and the second group included *Q. ilex* (9.5 μm) and *M. grandiflora* (9.9 μm; Table 3).

Citrus × *aurantium* had glabrous leaves, whereas the remaining species ranked according to trichome number per leaf surface area (N_t, m^{-2}) as: *Q. ilex* < *M. grandiflora*, *C. humilis* = *M. grandiflora* and *C. humilis* = *Q. ilex* (Table 3 and Fig. 2). *Chamaerops humilis* and *M. grandiflora* had filiform trichomes, hooked filiform in *M. grandiflora* and uniseriate filiform in *C. humilis* (Fig. 2). *Quercus ilex* had stellate trichomes (Fig. 2). The increase in trichome complexity in *Q. ilex* is reflected in the highest surface area of trichomes per leaf area (S_t, m^2 m^{-2}, 8.25 m^2 m^{-2}, Table 3). *Magnolia grandiflora* was similar to *Q. ilex* (= 7.34 m^2 m^{-2}), and *C. humilis* had the lowest S_t (4.88 m^2 m^{-2}; Table 3).

3.2. Spectroscopic characterization of leaf surface and esterification index

Although similar in term of the position (wavenumbers) of the main absorption bands in the infrared spectra, relative intensities of different absorption bands in *C. humilis*, *C.* × *aurantium*, *M. grandiflora* and *Q. ilex* had characteristic signatures and allowed species distinction; this reflected species differences in leaf surface functional traits and different structural arrangements of leaf components (Fig. 3 and Table S2 in Supplementary Information).

In all species, a broad absorption band between 3334 and 3393 cm^{-1} was present, attributable to the stretching vibration of hydroxyl groups

Table 3 –
Average (± SE) leaf surface functional traits in the four studied tree species.

	Stomatal characteristics				Cuticle characteristics				Trichome characteristics	
	$N_{s,l}$ (m^{-2})	$N_{s,u}$ (m^{-2})	S_s (m^2m^{-2})	S_{sp} (m^2m^{-2})	$T_{c,l}$ (μm)	$T_{c,u}$ (μm)	E_l	E_u	$N_{t,l}$ (m^{-2})	S_t (m^2m^{-2})
Chamaerops humilis	2.22 10^8 ± 3.5 10^6 ^{a}	0.701 10^8 ± 4.3 10^6	0.068 ± 0.0011^{ab}	0.0204 ± 0.0003^a	5.37 ± 0.13^a	6.59 ± 0.26^a	0.2970 ± 0.0037^a	0.297 ± 0.008^{ab}	1.62 10^8 ± 2.9 10^6 ^{ab}	4.88 ± 0.13^a
Citrus × *aurantium*	2.62 10^8 ± 1.4 10^6 ^{a}	np	0.0542 ± 0.0006^a	0.0084 ± 0.0001^b	3.63 ± 0.08^b	5.02 ± 0.17^a	0.413 ± 0.016^{ab}	0.342 ± 0.025^a	np	np
Magnolia grandiflora	2.80 10^8 ± 2.7 10^{6a}	np	0.0955 ± 0.0014^{ab}	0.0118 ± 0.0002^b	nd	9.92 ± 0.24^b	0.545 ± 0.016^{ab}	0.320 ± 0.012^a	1.84 10^8 ± 4.6 10^6 ^{a}	7.34 ± 0.25^b
Quercus ilex	3.91 10^8 ± 2.2 10^{6b}	np	0.1461 ± 0.0010^b	0.0165 ± 0.0002^{ab}	5.08 ± 0.21^a	9.50 ± 0.20^b	0.677 ± 0.082^b	0.239 ± 0.0041^b	1.41 10^8 ± 2.1 10^6 ^{b}	8.25 ± 0.14^b

Stomatal characteristics include number of stomata on lower ($N_{s,l}$) and upper surface ($N_{s,u}$), surface of stomatal area per leaf area (S_s) and surface of stomatal pore area per leaf area (S_{sp}); cuticle characteristics include thickness of cuticle of lower ($T_{c,l}$) and upper leaf surface ($T_{c,u}$) and esterification index of lower and upper surface (E_l and E_u); trichome characteristics are number of trichomes on lower surface ($N_{t,l}$) and surface area of trichomes per leaf area (S_t). $n = 30$ for $N_{s,l}$, $N_{s,u}$, S_s, S_{sp}, $T_{c,l}$, $T_{c,u}$, $N_{t,l}$ and N_t; $n = 10$ for E_l and E_u). Different letters indicate significant differences among species ($p < 0.05$). nd - not detectable, np - not present.

(Table S2 in Supplementary Information). This band was particularly emphasized in the lower surface of *Q. ilex* and *M. grandiflora* (Fig. 3). The spectra in all species also had characteristic bands at ca. 2916 and 2848 cm^{-1} that describe the asymmetrical stretching vibrations and symmetrical stretching vibrations of methylene groups and attributable to the presence of waxes and cutin (Table S2 in Supplementary Information). In contrast to the other samples, only the surfaces of *C. humilis* (both upper and lower) and *Q. ilex* (upper only) showed the presence of a band between 2954 and 2953 cm^{-1} attributable to waxes (Table S2 in Supplementary Information). In all the samples, two well-defined doublets at ca. 1470–1460 cm^{-1} and 730–720 cm^{-1}, attributable to CH_2 aliphatic bending vibrations, were observed (Fig. 3 and Table S2 in Supplementary Information). These bands show the presence of epicuticular and intracuticular waxes (Table S2 in Supplementary Information).

Occurrence of three very weak bands attributable to C–C stretching vibrations in aromatic compounds in upper and lower surfaces of *C. humilis* suggested presence of phenolic compounds in surface structures in this species (Table S2 in Supplementary Information). The upper surfaces of *C.* × *aurantium*, *M. grandiflora* and *Q. ilex* had only one weak band attributable to C-C stretching vibrations in aromatic compounds (Table S2 in Supplementary Information). Upper and lower surfaces of *M. grandiflora* and lower surface of *Q. ilex* exhibited strong absorption peaks in the spectral region 1300–900 cm^{-1} shared by polysaccharides and cutin (Fig. 3 and Table S2 in Supplementary Information).

The esterification index for lower leaf side (E_l) ranged from 0.68 to 0.28, while that for upper leaf side (E_u) varied from 0.34 to 0.24 (Table 2). *Quercus ilex* had the highest E_l value, and the lowest E_u value (Table 2). The highest E_u value was observed for *C.* × *aurantium* (Table 2). E_l and E_u values were numerically similar for *C. humilis* and *C.* × *aurantium* (Table 2).

3.3. Air pollution and weather conditions

PM concentration levels were similar for each sampling date during the entire exposure period (coefficient of variation < 35%, Huang et al., 2015; Table S3 and S4 in Supplementary File). Therefore, average concentration of pollutants was used to characterize air pollution conditions over the entire period for each ARPAC station (www.arpacampania.it). The monthly average (± SD) temperature was 27.4 ± 1.1 °C, the average (± SD) wind speed was 2.8 ± 0.05 m s^{-1}, the main wind direction was west, and there was no precipitation during the entire period.

3.4. Concentrations and accumulation rates of PM and PAHs

3.4.1. Particulate matter

At the first day of sampling in August, PM_{10} concentration estimated from distilled water extracts were the highest *M. grandiflora* and *C. humilis*, followed by *C.* × *aurantium* and *Q. ilex* (Table 4). The subsequent extraction with chloroform showed the highest concentration of PM_{10} in *Q. ilex* and *C. humilis* and the lowest in *C.* × *aurantium*. According to the total amount of coarse particulate matter (sum of distilled water and chloroform extracts), the species were ordered as: *Q. ilex* = *C. humilis* = *M. grandiflora* > *C.* × *aurantium*. One month later, *C. humilis* and *Q. ilex* showed the highest PM_{10} concentration estimated from distilled water extract, *M. grandiflora* and *Q. ilex* the highest concentration after chloroform extraction, and *C.* × *aurantium* samples had the lowest PM_{10} concentrations for both extractions. The species ordered according to the PM_{10} concentrations the same way in August and September (Table 4). As the result, species ranked the same way according to values of daily uptake rate of coarse particulate matter (U_{PM10}): *Citrus* × *aurantium* had the smallest U_{PM10}, and *Q. ilex, C. humilis* and *M. grandiflora* the largest. The ratio of particulate matter extracted with chloroform to total uptake (Θ_{PM10}) was similar among the species; the only difference was a moderately higher value of *Q. ilex* compared with *C.* × *aurantium* (Table 4).

In August, concentration of fine particles ($PM_{2.5}$) estimated in distilled water extractions was higher in the leaves of *C.* × *aurantium*, *C. humilis* and *M. grandiflora* than in the leaves of *Q. ilex* (Table 5). Chloroform extractions showed highest $PM_{2.5}$ concentrations in *M. grandiflora* and *Q. ilex*, where the amounts of $PM_{2.5}$ exceeded those of *Q. ilex* by around four times and those of *C.* × *aurantium* and *C. humilis* by around ten and thirty times respectively (Table 5). The total concentration of PM2.5 extracted from the samples in D_0 reflected the order in which the species were found when considering the chloroform extraction alone (Table 5). In September, *M. grandiflora* leaves showed the highest concentrations of water-extracted $PM_{2.5}$, while for chloroform extraction the species were sorted as: *C. humilis* = *M. grandiflora* and *C. humilis* > *Q. ilex* = *C. aurantium* (Table 5). Considering the total $PM_{2.5}$ extracted from the samples in D_1, *M. grandiflora* had the highest concentration, higher than *C. humilis*, while *Q. ilex* and *C.* × *aurantium* showed lower concentrations (Table 5). Leaves of *C. humilis* had the highest daily uptake rate of fine particulate matter ($U_{PM2.5}$) (Table 5). The ratio of $PM_{2.5}$ in chloroform extract to total ($\Theta_{PM2.5}$) did not differ among species (Table 5).

3.4.2. Polycyclic aromatic hydrocarbons (PAHs) in intact leaves

At the first sampling date (D_0), *C. humilis* had four times greater concentration of low molecular mass PAH in intact leaves ($C_{LMM,D0,i}$) than *Q. ilex*, and an order of magnitude greater concentration than that in *M. grandiflora* and *C.* × *aurantium* (Table 6). *Citrus* × *aurantium* and *C. humilis* had the greatest concentration of medium molecular mass PAH in intact leaves ($C_{MMM,D0,i}$) (Table 6). The concentration of high molecular mass PAH in intact leaves ($C_{HMM,D0,i}$) was only detectable for *C.* × *aurantium* and *Q. ilex* (Table 6). Species were ranked according to the uptake rate of low molecular mass PAH ($U_{LMM,i}$) as *C.* × *aurantium* > *M. grandiflora* > *Q. ilex* and *C. humilis*, of daily uptake of medium molecular mass PAH ($U_{MMM,i}$) only in *M. grandiflora* and of daily uptake of high molecular mass PAH ($U_{HMM,i}$) in *Q. ilex* samples only (Table 6).

Table 4 –
Average (± SE) coarse particulate matter (PM_{10}) concentrations (C_{PM10}) at the start (D_0) and end (D_1) of the study, coarse particulate matter daily uptake rate (U_{PM10}) and the ratio between concentration of PM_{10} extracted with chloroform ($CHCl_3$) and total (water + chloroform extractions) concentration of PM_{10} (Θ_{PM10}) in the leaves of four investigated plant species.

	$C_{PM10,\ D0}$ (μg m^{-2})			$C_{PM10,\ D1}$ (μg m^{-2})				
	H_2O	$CHCl_3$	Total	H_2O	$CHCl_3$	Total	U_{PM10} (μg m^{-2} d^{-1})	Θ_{PM10}
Chamaerops humilis	965 ± 136^{a}	1112 ± 281^{a}	2077 ± 407^{a}	3018 ± 3^{a}	879 ± 13^{a}	3897 ± 14^{a}	61 ± 14^{a}	0.35 ± 0.06^{b}
Citrus × *aurantium*	982 ± 168^{ab}	105 ± 10^{b}	1087 ± 173^{b}	1201 ± 2^{b}	70 ± 21^{b}	1271 ± 22^{b}	6.1 ± 6.0^{b}	0.18 ± 0.01^{a}
Magnolia grandiflora	1512 ± 71^{a}	395 ± 3^{c}	1907 ± 71^{ab}	1711 ± 287^{ab}	1974 ± 504^{c}	3684 ± 360^{a}	59 ± 14^{a}	0.29 ± 0.07^{ab}
Quercus ilex	980 ± 21^{b}	1047 ± 358^{a}	2026 ± 344^{a}	2934 ± 25^{a}	1238 ± 88^{ac}	4172 ± 90^{a}	72 ± 11^{a}	0.36 ± 0.06^{b}

Symbols as: $C_{PM10,D0}$ – concentration of coarse particulate matter in leaves sampled in August; $C_{PM10,D1}$ – concentration of coarse particulate matter in leaves sampled in September; U_{PM10} - daily accumulation rate of coarse particulate matter; Θ_{PM10} - ratio between concentration of PM_{10} extracted with chloroform and total concentration of PM_{10}. Different letters indicate significant differences among species ($n = 4$; $p < 0.05$).

Table 5 –
Average (± SE) fine particulate matter ($PM_{2.5}$) concentrations ($C_{PM2.5}$) at the start (D_0) and end (D_1) of the study, fine particulate matter daily uptake rate ($U_{PM2.5}$) and ratio between concentration of $PM_{2.5}$ extracted with chloroform ($CHCl_3$) and total concentration of $PM_{2.5}$ ($\Theta_{PM2.5}$) in the leaves of the four investigated species.

Species	$C_{PM2.5,D0}$ (μg m^{-2})			$C_{PM2.5,D1}$ (μg m^{-2})			$U_{PM2.5}$ (μg m^{-2} d^{-1})	$\Theta_{PM2.5}$
	H_2O	$CHCl_3$	Total	H_2O	$CHCl_3$	Total		
C. humilis	218 ± 37^a	198 ± 75^a	416 ± 63^a	166 ± 15^a	1009 ± 172^a	1176 ± 182^a	25.3 ± 7.9^a	0.65 ± 0.09
C. × *aurantium*	168 ± 73^a	193 ± 21^a	361 ± 70^a	260 ± 9^a	140 ± 36^b	400 ± 40^b	1.3 ± 2.4^b	0.47 ± 0.08
M. grandiflora	174 ± 26^a	1934 ± 76^b	2102 ± 74^b	516 ± 214^b	878 ± 216^{ab}	1394 ± 91^c	2.9 ± 4.2^b	0.84 ± 0.05
Q. ilex	107 ± 12^b	612 ± 110^b	719 ± 105^c	229 ± 33^a	523 ± 153^b	753 ± 140^b	1.1 ± 6.8^b	0.75 ± 0.05

Symbols as: $C_{PM2.5,D0}$ – concentration of fine particulate matter in leaves sampled in August; $C_{PM2.5,D1}$ - concentration of fine particulate matter in leaves sampled in September; $U_{PM2.5}$ - daily accumulation rate of fine particulate matter; $\Theta_{PM2.5}$ - ratio between concentration of $PM_{2.5}$ extracted with chloroform and total (water + chloroform extractions) concentration of $PM_{2.5}$. Different letters indicate statistically significant differences among species ($n = 4$; $p < 0.05$).

3.4.3. Polycyclic aromatic hydrocarbons (PAHs) in dewaxed leaves

Analysis of dewaxed leaves provides information of the amount of PAHs translocated into and accumulated in the subcuticular tissues and in cuticular and trichome hydrophilic regions over a 30-day period (Table 7). Overall, the PAH concentrations in dewaxed leaves were low, indicating that these pollutants accumulated mainly in the cuticular hydrophobic layer (Table 7). The differences between the concentrations of intact and dewaxed leaves indicated that *C. humilis* and *M. grandiflora* were the species with the highest $U_{LMM,dw}$ and $U_{MMM,dw}$ (Table 7). In none of the considered species, $U_{HMM,dw}$ exceeded the detection limit (Table 7).

3.5. Relationships among pollutant concentrations and uptake rates

Concentration and daily uptake rate of PM_{10} (C_{PM10} and U_{PM10}) were positively correlated. Θ_{PM10} and $\Theta_{PM2.5}$, that characterize the contribution of particulate matter stored in leaf hydrophobic phase were positively related with the concentrations of coarse and fine PM, and both Θ_{PM10} and $\Theta_{PM2.5}$ were positively related with the daily uptake of the coarse particulate matter (U_{PM10}) (Fig. 4). C_{PM10} was negatively correlated with concentration of medium molecular mass compounds in dewaxed leaves ($C_{MMM,dw}$) and the uptake rates of low and medium molecular mass compounds in intact leaves ($U_{LMM,i}$ and $U_{MMM,i}$) (Fig. 4). For intact leaves, the concentrations of low, medium and high molecular mass compounds ($C_{LMM,i}$, $C_{MMM,i}$ and $C_{HMM,i}$) were positively correlated with the uptake rates of corresponding pollutants ($U_{LMM,i}$, $U_{MMM,i}$ and $U_{HMM,i}$) (Fig. 4). $C_{MMM,i}$ and $C_{HMM,i}$ were positively correlated with the concentrations of MMM and HMM in dewaxed leaves ($C_{MMM,dw}$ and $C_{HMM,dw}$) (Fig. 4). $C_{MMM,dw}$ was positively correlated with the uptake rates of MMM in both intact and dewaxed leaves ($U_{MMM,i}$ and $U_{MMM,dw}$) (Fig. 4).

3.6. Correlations of leaf surface functional traits with pollutant uptake

Number of stomata on lower leaf side ($N_{s,l}$) and esterification index of the lower leaf side (E_l) were positively correlated (Fig. 4). Stomatal surface area per leaf area (S_s) was positively correlated with $N_{s,l}$, E_l, thickness of cuticle in upper leaf side ($T_{c,u}$), and the surface of trichomes per leaf area (S_t); moreover, S_s showed a negative correlation with the esterification index of upper leaf side (E_u) (Fig. 4). Upper cuticle thickness ($T_{c,u}$) showed positive correlations with trichome surface per leaf area (S_t) and number (N_t) (Fig. 4).

Stomatal surface area per leaf area (S_s) and the number and surface area trichomes per leaf area (N_t and S_t) showed strong positive correlations with the concentration of coarse particulate matter (C_{PM10}; Fig. 4). Stomatal pore area per leaf area (S_{sp}), N_t and S_t and the thickness of cuticle of the upper leaf side ($T_{c,u}$) were positively correlated with coarse particulate matter uptake rate (U_{PM10}; Fig. 4). In addition, S_s, S_{sp} were positively correlated with the share of hydrophobic PM_{10} accumulation (Θ_{PM10}), and $T_{c,u}$ and N_t and S_t were positively correlated with both Θ_{PM10} and $\Theta_{PM2.5}$ (Fig. 4).

Esterification index of lower leaf surface (E_l), S_s and $N_{s,l}$ were positively correlated with concentration of HMM PAH in intact and dewaxed leaves ($C_{HMM,i}$ and $C_{HMM,dw}$), and with daily uptake of HMM PAH in intact leaves ($U_{HMM,i}$), but esterification index of upper leaf side (E_u) was negatively correlation with HMM PAH concentration and uptake (Fig. 4).

3.7. Clustering of species according to functional traits and pollutant uptake

Different suites of functional traits clearly separated the species in the PCA space (Fig. 5A). The esterification index of the upper leaf side (E_u) determined the clustering of *C.* × *aurantium* samples (Fig. 5A).

Table 6 –
Average (± SE) concentrations (C, μg m^{-2}) and daily accumulation rate (U, μg m^{-2} d^{-1}) of low (LMM), medium (MMM) and high (HMM) molecular mass PAHs found in intact leaves (i) of the four investigated plant species at D_0 and D_1.

Species	$C_{LMM,D0,i}$ (μg m^{-2})	$C_{LMM,D1,i}$ (μg m^{-2})	$U_{LMM,i}$ (μg m^{-2} d^{-1})	$C_{MMM,D0,i}$ (μg m^{-2})	$C_{MMM,D1,i}$ (μg m^{-2})	$U_{MMM,i}$ (μg m^{-2} d^{-1})	$C_{HMM,D0,i}$ (μg m^{-2})	$C_{HMM,D1,i}$ (μg m^{-2})	$U_{HMM,i}$ (μg m^{-2} d^{-1})
C. humilis	2.75 ± 0.645^a	2.59 ± 0.881^a	nd^a	0.327 ± 0.125^a	0.318 ± 0.118^a	nd^a	<IDL^a	<IDL^a	nd^a
C. × *aurantium*	0.416 ± 0.191^c	2.39 ± 1.45^a	0.065 ± 0.045^b	2.24 ± 1.01^b	1.04 ± 0.445^b	nd^a	0.0787 ± 0.0324^b	<IDL^a	nd^a
M. grandiflora	0.225 ± 0.116^c	0.424 ± 0.151^b	0.0066 ± 0.0027^c	0.339 ± 0.167^a	0.595 ± 0.227^a	0.0085 ± 0.0117^b	<IDL^a	<IDL^a	nd^a
Q. ilex	0.773 ± 0.283^b	0.343 ± 0.120^b	nd^a	1.03 ± 0.272^{ab}	0.640 ± 0.0356^a	nd^a	0.0299 ± 0.00348^b	0.281 ± 0.0386^b	0.0083 ± 0.0012^b

Symbols as: $C_{LMM,D0,i}$ – concentration of low molecular mass PAH in intact leaves sampled at D_0; $C_{LMM,D1,i}$ – concentration of low molecular mass PAH in intact leaves sampled at D_1; $U_{LMM,i}$ – daily uptake rate of low molecular mass PAH in intact leaves; $C_{MMM,D0,i}$ – concentration of medium molecular mass PAH in intact leaves sampled at D_0; $C_{MMM,D1,i}$ – concentration of medium molecular mass PAH in intact leaves sampled at D_1; $U_{MMM,i}$ – daily uptake rate of medium molecular mass PAH in intact leaves; $C_{HMM,D0,i}$ – concentration of high molecular mass PAH in intact leaves sampled at D_0; $C_{HMM,D1,i}$ – concentration of high molecular mass PAH in intact leaves sampled at D_1; $U_{HMM,i}$ – daily uptake rate of high molecular mass PAH in intact leaves. IDL is the instrumental detection limit (< 0.007 μg m^{-2}). When there was no uptake, or uptake could not be calculated due to too low PAH concentration (<IDL), it was reported as non-detectable (nd). Different letters indicate statistically significant differences among species ($n = 4$; $p < 0.05$).

Table 7 –
Average (± SE) concentrations (C, μg m^{-2}) and daily accumulation rate (U, μg m^{-2} d^{-1}) of low (LMM), medium (MMM) and high (HMM) molecular mass PAHs in dewaxed leaves (dw) of the four investigated plant species at the start (D_0) and end (D_1) of the study.

Species	$C_{LMM,D0,dw}$ (μg m^{-2})	$C_{LMM,D1,dw}$ (μg m^{-2})	$U_{LMM,dw}$ (μg m^{-2} d^{-1})	$C_{MMM,D0,dw}$ (μg m^{-2})	$C_{MMM,D1,dw}$ (μg m^{-2})	$U_{MMM,dw}$ (μg m^{-2} d^{-1})	$C_{HMM,D0,dw}$ (μg m^{-2})	$C_{HMM,D1,dw}$ (μg m^{-2})	$U_{HMM,dw}$ (μg m^{-2} d^{-1})
C. humilis	<IDL[a]	0.075 ± 0.038[a]	0.0024 ± 0.0013[a]	0.015 ± 0.0032[a]	0.031 ± 0.0086[a]	0.00053 ± 0.00023[a]	<IDL[a]	<IDL[a]	nd
C. × *aurantium*	0.106 ± 0.0335[b]	0.045 ± 0.015[a]	nd[b]	2.44 ± 0.924[b]	0.31 ± 0.095[b]	nd[b]	<IDL[a]	<IDL[a]	nd
M. grandiflora	0.059 ± 0.0072[c]	0.046 ± 0.017[a]	nd[b]	0.13 ± 0.053[c]	0.17 ± 0.045[b]	0.0013 ± 0.0026[a]	<IDL[a]	<IDL[a]	nd
Q. ilex	1.26 ± 0.604[b]	0.090 ± 0.031[a]	nd[b]	0.36 ± 0.13[c]	0.15 ± 0.077[b]	nd[b]	0.048 ± 0.0020[b]	0.015 ± 0.0088[b]	nd

Symbols as: $C_{LMM,D0,dw}$ – concentration of low molecular mass PAH in dewaxed leaves sampled at D_0; $C_{LMM,D1,dw}$ – concentration of low molecular mass PAH in dewaxed leaves sampled at D_1; $U_{LMM,dw}$ – daily uptake rate of low molecular mass PAH in dewaxed leaves; $C_{MMM,D0,dw}$ – concentration of medium molecular mass PAH in dewaxed leaves sampled at D_0; $C_{MMM,D1,dw}$ – concentration of medium molecular mass PAH in dewaxed leaves sampled at D_1; $U_{MMM,dw}$ – daily uptake rate of medium molecular mass PAH in dewaxed leaves; $C_{HMM,D0,dw}$ – concentration of high molecular mass PAH in dewaxed leaves sampled at D_0; $C_{HMM,D1,dw}$ – concentration of high molecular mass PAH in dewaxed leaves sampled at D_1; $U_{HMM,dw}$ – daily uptake rate of high molecular mass PAH in dewaxed leaves. IDL is the instrumental detection limit (< 0.007 μg m^{-2}). When no uptake was observed, or the uptake rate could not be calculated due to low PAH concentrations (below IDL), U was reported as non-detectable (nd). Different letters indicate statistically significant differences among species ($n = 4$; $p < 0.05$).

Chamaerops humilis was distinguished by the number of stomata on the upper leaf side ($N_{s,u}$), the surface of stomatal pore area per leaf area (S_{sp}) and the thickness of cuticle of lower leaf side ($T_{c,l}$) (Fig. 5A). The traits separating *M. grandiflora* and *Q. ilex* were esterification index of lower leaf side (E_l), number of stomata on lower leaf side ($N_{s,l}$), thickness of cuticle on upper leaf side ($T_{c,u}$) and stomatal surface area per leaf area (S_s) (Fig. 5A). The remaining functional traits (surface of trichomes per leaf area – S_t; number of trichomes – N_t) were in an intermediate position between the samples of *Q. ilex*, *M. grandiflora* and *C. humilis*, but the samples *C.* × *aurantium* had lower values for these traits than the other species (Fig. 5A).

According to pollutant concentrations and uptake rates, *C. humilis* and *M. grandiflora* were grouped together mainly as the result of similar $C_{PM2.5}$ and $U_{PM2.5}$ (Fig. 5B). *Quercus ilex* was separated from other species as the result of higher concentration of high molecular mass PAHs in intact and dewaxed leaves ($C_{HMM,i}$ and $C_{HMM,dw}$) and the daily uptake of high molecular mass PAHs in intact leaves ($U_{HMM,i}$). The concentration and uptake of PM_{10} (C_{PM10} and U_{PM10}) and the ratio between the particulate matter extracted with chloroform to total extracted ($\Theta_{PM2.5}$ and Θ_{PM10}), were in an intermediate position between the samples of *Q. ilex*, *M. grandiflora* and *C. humilis*. (Fig. 5B). Clustering of *C.* × *aurantium* was primarily determined by PC2 that primarily depended on concentration and uptake of low and medium molecular mass PAHs in intact and dewaxed leaves ($C_{LMM,i}$, $U_{LMM,i}$, $C_{LMM,dw}$, $U_{LMM,dw}$, $C_{MMM,i}$, $U_{MMM,i}$, $C_{MMM,dw}$, $U_{MMM,dw}$), but also depended on the negative correlations with C_{PM10}, U_{PM10}, $\Theta_{PM2.5}$ and Θ_{PM10} on the same principal component (Fig. 5B).

PCA using both functional traits, and pollutant concentrations and uptake rates resulted in similar separation of species (Fig. 5C). Highlighted on the first principal component two main groups: (i) a first one corresponding to concentration and uptake rate of MMM PAH in intact and dewaxed leaves ($C_{MMM,i}$, $C_{MMM,dw}$, $U_{MMM,dw}$, $U_{MMM,i}$),concentration of LMM PAH in dewaxed leaves ($C_{MMM,dw}$) and esterification index of upper leaf side (E_u) and (ii) a second one featured by U_{PM10}, S_t, $T_{c,u}$, C_{PM10}, S_{sp}, N_t, $\Theta_{PM2.5}$ and Θ_{PM10} (Fig. 5C). *Citrus* × *aurantium* samples were located near to the variables of first group according to the PCA area (Fig. 5C). The vector depicting the concentration of fine particulate matter in the air ($C_{PM2.5,a}$) is also projected on the same axis, although detached from *C.* × *aurantium* (Fig. 5C). The second group of variables mainly describes the characteristics of *M. grandiflora* and partially those of *Q. ilex*, being in an intermediate position between the two species (Fig. 5C).

The second principal component (PC2) explained 23.8% of data and, also in this case, it were possible observe two different groups of variables: (i) the first group was formed by the number of stomata on upper leaf surface ($N_{s,u}$) and the uptake rate of $PM_{2.5}$ ($U_{PM2.5}$); (ii) the second group was characterized by the presence of concentration and uptake of HMM PAH ($C_{HMM,i}$, $C_{HMM,dw}$ and $U_{HMM,i}$), number on lower leaf side and surface of stomata ($N_{s,l}$ and S_s), and the esterification index of lower leaf side (E_l, Fig. 5C).

These two groups separated *Q. ilex* from *C. humilis* species (Fig. 5C). *Chamaerops humilis* samples were near of the $N_{s,u}$ and $U_{PM2.5}$ vectors tightly clustered together (Fig. 5C). The second group of variables completed the description of *Q. ilex* (Fig. 5C).

4. Discussion

4.1. Leaf surface structural traits

The functional traits of plants reflect plant adaptive response to their growth environment, and thus, species in the same biome often share similar traits (Reich et al., 1999; Bu et al., 2019; Wright et al., 2004). The marked seasonality of the Mediterranean climate makes this ecosystem very peculiar and has resulted in a specific suite of traits including evergreen sclerophyllous leaves that often have a thick trichome layer on the lower leaf surface, but sometimes also on both leaf surfaces (Niinemets and Keenan, 2014; Niinemets et al., 2004; Yadav et al., 2004; La Riva et al., 2018). Yadav et al. (2004) measured stomatal, trichome and cuticle traits in eight Mediterranean species with evergreen sclerophyllous leaf habit, and demonstrated that these species presented marked presence of these traits as adaptation strategies to summer drought. In this study, we analyzed the variation of stomatal, cuticle and trichome traits (Table 1) in four widespread Mediterranean species assess the role of these traits in altering the capacity to capture particulate matter and PAHs as has been shown for several other species (Łukowski et al., 2020; Zhang et al., 2018).

In our study, stomatal number per area varied from 222 stomata mm^{-2} in *C. humilis* to 391 stomata mm^{-2} in *Q. ilex* (Table 3) in line with previous work in the Mediterranean flora, where the number of stomata ranged from 250 to 500 stomata mm^{-2} (Bosabalidis and Kofidis, 2002; Yadav et al., 2004; Deng et al., 2017). Furthermore, species strongly differed in the leaf area covered by stomatal pores and entire stomata (Table 3 and Fig. 2). Stomatal area per leaf area is less frequently measured than stomatal size and number, but we argue that this trait more readily describes the area available for diffusion of pollutants into leaf interior. Only *C. humilis* was amphistomatous (Table 3 and Fig. 2). This feature is an ancient trait characteristic to the species from family Arecaceae as an evolutionary adaptation to hot and humid climate during their diversification in Oligocene (Wang et al., 2015; Song et al., 2021).

The trichome area (S_t) of *Q. ilex* exceeded the projected leaf area by a factor of more than eight (Table 3). This high trichome surface area

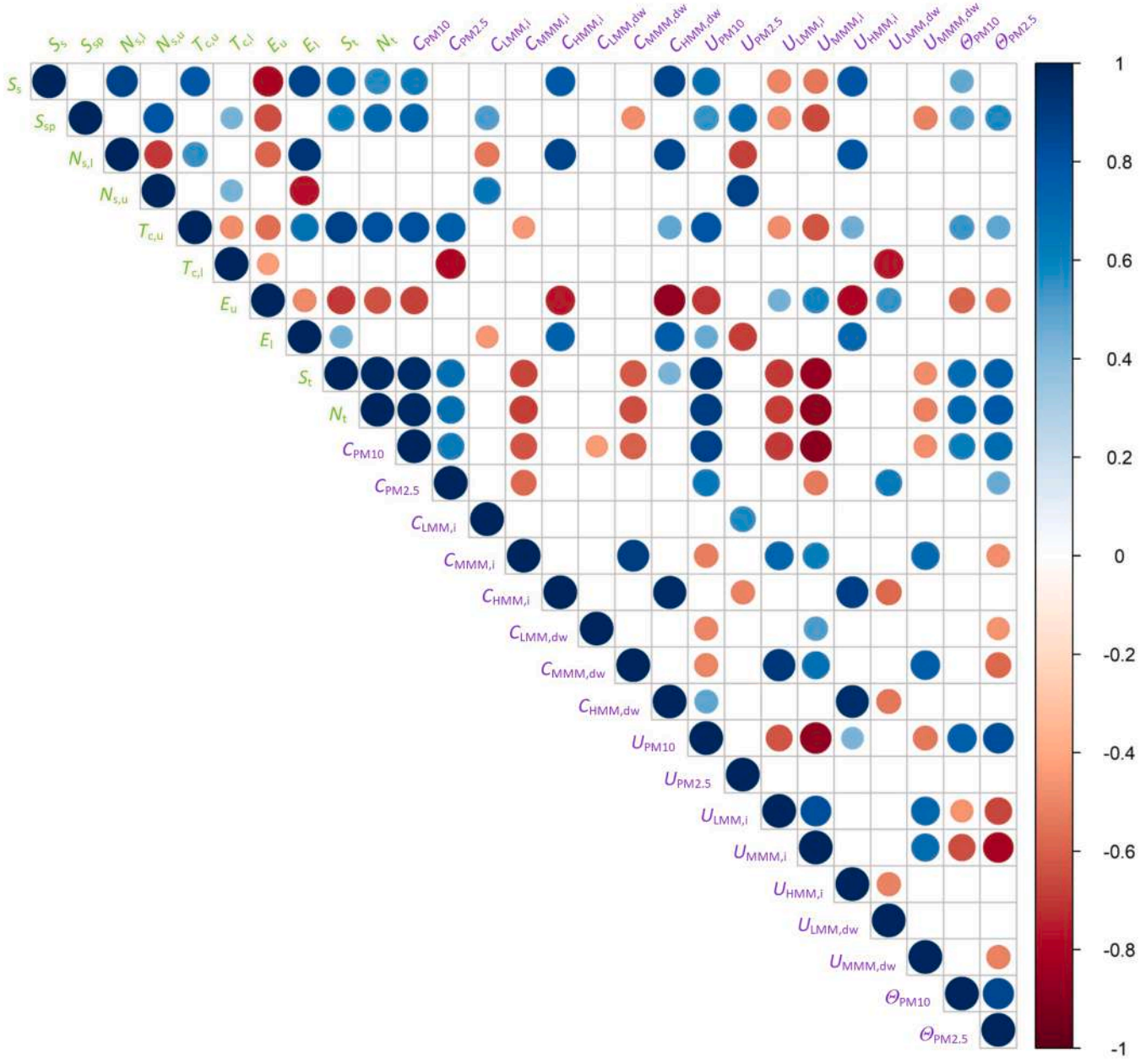

Fig. 4. – Correlation matrix of leaf surface functional traits and pollutants concentrations and daily uptake rates. The color intensity (light to dark) and the size of the circle (small to big) are proportional to the Spearman correlation coefficients (0 to 1 for the positive coefficient and 0 to −1 for negative coefficient). Only significant correlations ($p < 0.05$) are shown. Daily uptake of HMM in dewaxed leaves ($U_{HMM,dw}$) was not included in the analysis because it was below the detection limit (Table 7). All symbols are defined in Table 1.

reflects the greater area of stellate trichomes in *Q. ilex* (Fig. 2; Deng et al., 2017). Nevertheless, in *M. grandiflora* and *C. humilis* that have non-branched filiform trichomes, S_t was also high, between 4.88 and 7.34 m^2m^{-2} (Table 3). Overall, the three species with trichomatous leaves had a higher number of trichomes on the lower leaf side ($N_{t,l}$) than the Mediterranean species on average (Yadav et al., 2004). High trichome number might also indicate plastic adjustment of trichome density to polluted environments as has been observed in other studies (Pal et al., 2002; Balasooriya et al., 2009; Kardel, Kováts et al., 2010, 2021).

Cuticle thickness of lower and upper leaf sides ($T_{c,l}$ and $T_{c,u}$) observed in this study (Table 3) was within the range of values found by Yadav et al. (2004) for other Mediterranean species. Our study also confirmed the greater thickness of the upper cuticle (Table 3). The cuticle characteristics indicated that leaves of *C.* × *aurantium* and *C. humilis* could be considered equifacial, while the leaves of *Q. ilex* and *M. grandiflora* showed a pronounced bifaciality, because of more pronounced differences in thickness of the lower and upper cuticles (Table 3).

In our study, S_S scaled positively with upper cuticle thickness and S_t and S_t and upper cuticle thickness were also positively correlated (Fig. 4). These correlations complicate interpretation of the correlations between leaf surface characteristics and pollutant uptake rates as discussed in Section 4.4.

4.2. Leaf surface chemistry

Infrared spectra of fresh leaf surfaces displayed variable fingerprints of the intensity of absorption bands due to the complex assemblage of leaf components (Heredia-Guerrero et al., 2014), and displayed the

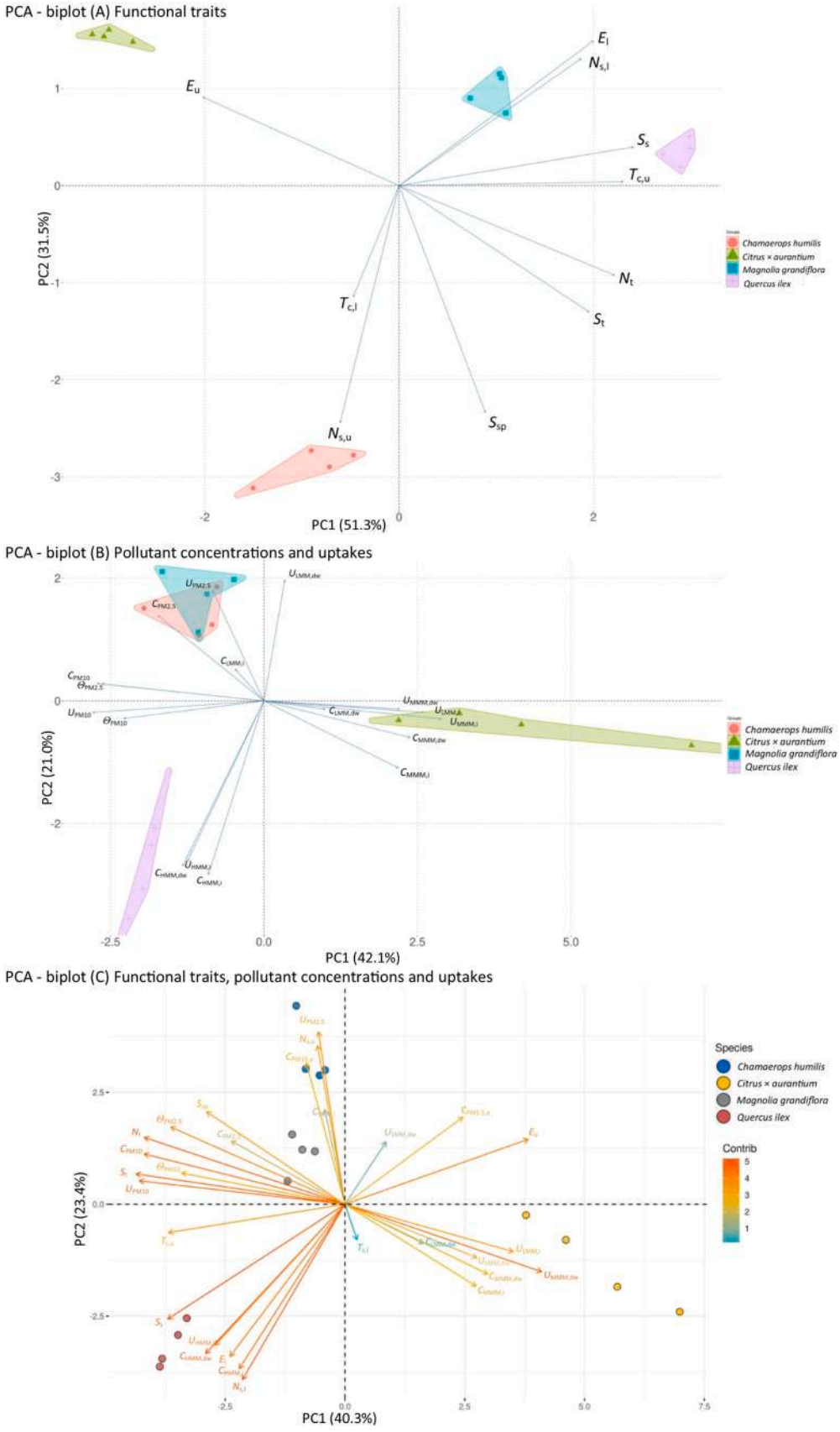

Fig. 5. – The PCA biplot is a 2D graphical representation that shows associations between observations (plant samples) and the traits. The lengths of the rays are directly proportional to the variance of the corresponding variable included in the two components displayed, while angle between the vectors indicate the strength of correlation between them (Zuzolo et al., 2020). Biplots of principal component analyses (PCA) biplot showing (A) the ordination of species in the PCA space determined by leaf functional traits and contributions of leaf surface functional traits of trichomes, cuticle and stomata to the PCA axes; (B) ordination of species in the PCA space determined by pollutant concentrations (C) and uptake rates (U) and the impact of different concentrations and uptake rates on PCA; (C) ordination of species in the PCA space determined by leaf surface functional traits, average pollutants concentrations and pollutants daily uptake rates and different contributions of traits to PCA axes. Plant samples and the included variables are expressed as symbols and vectors. The plots display the first (PC1) and second (PC2) principal components, variance explained by PC1 and PC2 and the variable contributions (as characterized by the length of the vectors) to the first two principal components. All symbols are defined in Table 1. The uptake rate of high molecular mass compounds in subcuticular tissues ($U_{HMM,dw}$) was not included in the PCA analyses as it was below the detection limit (Table 7).

distinctive spectral features of the main cuticle components such as cutin, waxes, polysaccharides and phenolic compounds (Da Luz, 2006, Fig. 3). Waxes (epi- and intracuticular), and polysaccharides are the most observable cuticle components in infrared spectra (Fig. 3 and Table S3 in Supplementary Information) (Izzo et al., 2020). The doublets attributable to CH_2 aliphatic bending vibrations (1470–1460 cm^{-1} and 730–720 cm^{-1}), found in all samples (Fig. 3 and Table S2), were identified as nanocosane, a compound already identified in the cuticle of the Mediterranean species *Olea europea* (Silverstein and Webster, 1998; Da Luz et al., 2006).

The differences in contribution of polysaccharides is clearly observed in the lower sides both of *Q. ilex* and *M. grandiflora*, whose pronounced bifaciality was confirmed by spectroscopic analysis (Fig. 3). A signal intensification in the bands at ca. 1030 cm^{-1} (related to the C–O–C stretching vibration of glycosydic bond in polysaccharides) was evident in lower surfaces of both the species (Fig. 3). Since the leaves were analyzed without removing the trichome layer from the lower surface, it was assumed that this peculiar spectral features of *Q. ilex* and *M. grandiflora* could be related to trichomes related leaf surface functional traits, accordingly with Da Luz et al. (2006) who have experienced increases in signal intensity in the 1031 cm^{-1} band caused by trichome layer on lower leaves surfaces. In fact, the lower surface of both *Q. ilex* and *M. grandiflora* showed high trichome density (N_t) and surface per leaf area (S_t) (Table 3) that could affect the identification of cuticle components and the resultant esterification indices (*E*). This aspect is also highlighted by the significant intensification of the broad bands at ca. 3400 cm^{-1} (Fig. 3) that is generally observed in both organic and inorganic compounds (Picariello et al., 2021; Izzo et al., 2020) but particularly emphasized in the presence of a polysaccharide fraction and, secondly, non-esterified hydroxyl groups of cutin (Heredia-Guerrero et al., 2014). Indeed, *E* was similar for the upper and lower cuticle in non-hairy *C.* × *aurantium*, but *E* was greater for the lower cuticle in *Q. ilex* and *M. grandiflora* (Table 3). However, *E* values were also similar for upper and lower leaf surface in the trichomatous species *C. humilis*.

The presence of waxes results in a peculiar enhancement in the relative intensity of asymmetrical (νa) and symmetrical (νs) stretching vibrations of methylene groups at ca. 2916 and 2848 cm^{-1}. These absorption bands, along with bending vibration $\delta(CH_2)$ (ca. 1317 cm^{-1}), are generally shared with cutin that, being the main polyester in the cuticle, is considered the specific compound responsible of the spectral features at ca. 1730 cm^{-1} (C═O stretching vibration in esters). The band related to the stretching vibrations of the ester bond found in *C. humilis* at 1735 cm^{-1} has been found in other species (Da Luz et al., 2006) and was identified in the presence of cutan as the major component of the cuticle, instead of cutin. The presence of cutan, unsaponifiable polymer made of polymethylene chains linked by ether bonds (Heredia, 2003; Da Luz et al., 2006) likely explains the lower value of the esterification index (*E*) in *C. humilis* compared with other species (Table 4).

4.3. Concentrations and daily uptake rates of pollutants

Coefficient of variation of coarse and fine PM concentration levels in atmosphere, for each sampling date, during the entire exposure period was less than 35%, and therefore, average concentrations were used. Atmospheric factors such as wind, moisture or rain can affect PM previously deposited on the surface of plants causing resuspension of up to 50% (McPherson et al., 1998; Mo et al., 2015). Climatic data for the thirty-day study period suggested that wind had no relevant impact on particle resuspension and also that no runoff from the leaf surface occurred due the absence of precipitation during the study (Mo et al., 2015). This is particularly evident for PM_{10} concentrations and uptake in the four species; there was a strong increase of PM_{10} over the study period and the species ranking according to PM_{10} concentration did not vary over the period considered (Table 4). Overall, the share of hydrophobic PM_{10} (Θ_{PM10}; 0.18–0.36, Table 4) and hydrophobic fine particulate matter ($\Theta_{PM2,5}$; 0.47–0.84, Table 5) were large. Leaf PM_{10} concentrations (C_{PM10}) and uptake (U_{PM10}) were positively correlated with Θ_{PM10} and leaf $PM_{2.5}$ concentrations scaled positively with $\Theta_{PM2,5}$ (Fig. 4). This implies that the hydrophobicity of the leaf surface, e.g. presence of waxes is expected to play an important role in retention of particulate matter (Dzierzanowski et al., 2011; Wang and Shi, 2021, see the next section). No correlation was found between concentrations of particulate matter in the air and concentrations and uptake of particulate matter in leaves (Fig. 5A), but the particle concentrations depended on leaf surface characteristics (next section).

The analysis of PAHs of the intact leaves (Table 6) allowed to quantify the pollutants present on the leaf surface (whether or not bound to the cuticle) together with those eventually translocated into the subcuticular tissues. Data on intact leaves showed that the highest concentrations of LMM were initially found on *C. humilis*, however, after 30 days, the concentrations in *C.* × *aurantium* and in *C. humilis* were similar, indicating a higher average daily uptake rate in *C.* × *aurantium* (Table 6). *Citrus* × *aurantium* also had the greatest MMM concentrations (Table 6). The heavier polycyclic hydrocarbon were significantly only retained by *Q. ilex*. (Table 6). In accordance with our findings, Fasani et al. (2016) found that a higher accumulation of three- and four-ring slowly diffusing PAHs is related to the accessibility of cuticular surface that is increased in the absence of trichomes. Several authors also suggested that cutin is the key contributor in PAH storage, avoiding their intratissue movement (Chen and Schnoor, 2009; Li et al., 2010; Mętrak et al., 2016; Shechter and Chefetz, 2008). This latter consideration supports the PAH concentrations in dewaxed leaves; the species with the highest uptake for LMM and MMM was *C. humilis* (Table 7) whose cuticle contains cutan instead of cutin enhancing its hydrophobic nature (Shechter and Chefetz, 2008).

4.4. Scaling of pollutant concentrations and daily uptake rates with leaf surface functional traits

In our study, the impact of stomatal traits on pollutant sequestration was weaker than in other studies (Kováts et al., 2021 and references therein). Counterintuitively, we observed positive correlations among S_s and uptake of concentration (C_{PM10}) and uptake rate (U_{PM10}) of coarse particulate matter (PM_{10}) and HMM fraction of PAH, but no correlations with smaller particles, $PM_{2.5}$ and lower molecular mass PAH that can more readily diffuse into leaf interior (Fig. 4). In fact, stomatal uptake of pollutants directly depends on stomatal openness (Fowler et al., 2009; Niinemets et al., 2014) that in turn is strongly controlled by plant water availability. In particular, in Mediterranean species, stomatal openness is typically low in summer due to drought (Lange et al., 1982; Niinemets and Keenan, 2014; Reichstein et al., 2002). As there was no precipitation during the study period, the plants sustained severe drought stress, implying a low stomatal conductance. Thus, the puzzling correlations between stomatal traits and pollutant uptake observed in our study might reflect the correlation of stomatal traits with other leaf functional characteristics, S_t and upper cuticle thickness (Section 4.1). Further studies during wet periods when stomata are open are needed to characterize the stomatal pollutant uptake capacity.

As predicted, C_{PM10} and U_{PM10} were positively correlated with S_t (Fig. 4). Glabrous leaves of *C.* × *aurantium* had the lowest uptake capacity for PM_{10}, but the hairiest leaves of *Q. ilex* had the highest uptake rate (Table 4). The values of C_{PM10} measured in our study for *Q. ilex* are the same order of magnitude as observed previously (Esposito et al., 2020; Sgrigna et al., 2015). *Chamaerops humilis* and *M. grandiflora* with intermediate S_t showed a medium potential to trap coarse particles. In addition, both coarse and fine particulate (C_{PM10} and $C_{PM2.5}$) leaf concentrations were correlated with upper cuticle thickness (Fig. 4). The share of hydrophobic PM_{10} and $PM_{2.5}$ scaled also positively with upper cuticle thickness (Fig. 4). As there is a certain pore fraction within plant cuticles (Schönherr, 2006; Tredenick et al., 2017), this might indicate that thicker cuticles have a greater pore fraction. At any rate, cuticular

traits were primarily associated with the hydrophobic particle fraction, and we conclude that the most influent trait, regard the sequestration of particles is the presence, density and surface area of trichomes (Table 3, Fig. 4).

So far, *Q. ilex* has been studied for its ability to sequester PAHs (De Nicola et al., 2005, 2011; Orecchio, 2007). The ability of *C.* × *aurantium* to accumulate low and medium molecular mass hydrocarbons has been evaluated and certified in other studies proposing to use plant leaves as a bioindicator of PAHs pollution (Fasani et al., 2016). Yet, there are few interspecific comparisons. In the case of PAH, there were only a few correlations. In particular, esterification index of the upper surface (E_u) was negatively associated with high molecular mass (HMM) PAH concentrations and uptake (Fig. 4), suggesting that more strongly cross-linked fatty acids in cutin constitute a more effective barrier of HMM PAH. The low E_u of *C. humilis* (Table 3) could be the cause that allows pollutants to translocate into the subcuticular tissues due to the reduced influence of cutin (Chen and Schnoor, 2009; Li et al., 2010; Mętrak et al., 2016; Shechter and Chefetz, 2008). These support the hypothesis that hydrocarbons penetration into the leaf tissues is facilitated or slowed down depending on the chemical characteristics of the surface (Domínguez et al., 2015). HMM PAH concentrations were also positively related to S_s (Fig. 4), but these correlations likely reflected the negative association between S_s and E_u (Fig. 4). In the case of the esterification index of the lower cuticle (E_l), the relationships are non-conclusive because E_l was estimated with trichomes. Previously, it has been suggested that high trichome density allows pollutants to accumulate on trichome surface and prevent their penetration through the cuticle following the particle bound deposition (Jouraeva et al., 2003; Li et al., 2010; Domínguez et al., 2015). However, no correlations of PAH uptake were observed with trichome traits across species in our study (Fig. 4).

4.5. Species separation in functional traits and pollutant uptake space

High number and surface area of stomata and trichomes, together with thick upper cuticle characterized *Q. ilex* and *M. grandiflora* and justified their ability to concentrate PM_{10} with a high daily uptake (Fig. 5C). *Magnolia grandiflora* and *C. humilis* samples were grouped by their ability to uptake and retain fine particulate matter ($C_{PM2.5}$ and $U_{PM2.5}$) (Fig. 5B and C), however, no clear correlation was found between this capacity and the functional traits analyzed for these species. A direct correlation between $PM_{2.5}$ air concentration and PAHs concentrations was observed in other studies, since fine particulate matter act as a carrier of toxic organic compounds (Liu et al., 2017), but our study cannot assess this interaction (Fig. 5) due to the lack of PAHs atmospheric data.

Citrus × *aurantium* samples were clustered mainly due to strong negative correlations with trichome related traits and the index of hydrophobicity (Θ_{PM10} and $\Theta_{PM2.5}$) (Fig. 5A). In this species, high concentrations of LMM and MMM in intact and dewaxed leaves, high uptake of LMM and MMM in intact leaves and MMM in dewaxed leaves were observed (Fig. 5B and C).

5. Conclusions

This study provided new data of and novel insight into plant-air pollutant interactions, suggesting mechanisms that may prevent or promote translocation into leaf epidermis and non-hydrophobic regions. Our analyses uncovered a large variation in functional traits in key Mediterranean species, and demonstrated that several functional traits explain at least part of the interspecific variability in foliar accumulation of particulate matter and PAH. In particular, leaf hairiness, cuticular thickness and cuticular chemistry were found to be the main drivers explaining species differences. Trichomes can increase the surface by almost an order of magnitude and thus, they play a prominent role in phytoremediation. Previous studies have looked at the relationship between leaf shapes (Chen et al., 2017; Esposito et al., 2020), surface microstructures of the leaves (Zhang et al., 2018; Baraldi et al., 2019; Li et al., 2020), and their PM adsorption capacities, but there has been much less attention on the increase of surface for pollutant absorption due to trichomes. Light pollutants follow a different pathway of accumulation, interacting with the leaf mainly via stomata and cuticle. There is only limited information of what molecular and physical features of cuticle control lower molecular mass pollutant accumulation, including hydrophobicity, cross-linkage of cutin fatty acids and cutin porosity, and future efforts are needed to increase the knowledge base. This study proves that leaf surface functional traits deserve attention in air phytoremediation and Nature Based Solutions approaches. Given the interest in the results obtained and the perspectives to study the interaction between environment and leaves mediated by pertinent leaf functional traits, future research is needed to extend this work to more species. Species-specific data are especially needed to improve models that ca estimate vegetation capacity in air phytoremediation.

CRediT authorship contribution statement

Antonello Prigioniero: Investigation, Validation, Conceptualization and Writing - original draft. **Daniela Zuzolo:** Conceptualization, Visualization, Data curation and Formal analysis, Writing - Review & Editing. **Ülo Niinemets:** Validation, Supervision and Writing - Review & Editing. **Alessia Postiglione:** Investigation, Visualization. **Mariano Mercurio:** Investigation, Visualization. **Francesco Izzo:** Investigation, Visualization. **Marco Trifuoggi:** Investigation. **Maria Toscanesi:** Investigation. **Pierpaolo Scarano:** Data curation. **Maria Tartaglia:** Data curation. **Rosaria Sciarrillo:** Conceptualization and Supervision. **Carmine Guarino**: Conceptualization and Supervision.

Declaration of Competing Interest

The authors declare that they have no known competing financial interests or personal relationships that could have appeared to influence the work reported in this paper.

Appendix A. Supporting information

Supplementary data associated with this article can be found in the online version at doi:10.1016/j.jhazmat.2022.129029.

References

ARPAC, Campania Regional Environmental Protection Agency [WWW Document]. accessed on 2020 URL ⟨www.arpacampania.it⟩.

Balasooriya, B.L.W.K., Samson, R., Mbikwa, F., Vitharana, U.W.A., Boeckx, P., Van Meirvenne, M., 2009. Biomonitoring of urban habitat quality by anatomical and chemical leaf characteristics. Environ. Exp. Bot. 65 (2–3), 386–394. https://doi.org/10.1016/j.envexpbot.2008.11.009.

Baraldi, R., Chieco, C., Neri, L., Facini, O., Rapparini, F., Morrone, L., Rotondi, A., Carriero, G., 2019. An integrated study on air mitigation potential of urban vegetation: From a multi-trait approach to modeling. Urban For. Urban Green. 41, 127–138. https://doi.org/10.1016/j.ufug.2019.03.020.

Bosabalidis, A.M., Kofidis, G, 2002. Comparative effects of drought stress on leaf anatomy of two olive cultivars. Plant Sci. 163, 375–379. https://doi.org/10.1016/S0168-9452(02)00135-8.

Bu, W., Huang, J., Xu, H., Zang, R., Ding, Y., Li, Y., Lin, M., Wang, J., Zhang, C., 2019. Plant functional traits are the mediators in regulating effects of abiotic site conditions on aboveground carbon stock-evidence from a 30 ha tropical forest plot. Front. Plant Sci. 9, 1958. https://doi.org/10.3389/fpls.2018.01958.

Buda, G.J., Isaacson, T., Matas, A.J., Paolillo, D.J., Rose, J.K.C., 2009. Three-dimensional imaging of plant cuticle architecture using confocal scanning laser microscopy. Plant J 60, 378–385. https://doi.org/10.1111/j.1365-313X.2009.03960.x.

Chen, B., Schnoor, J.L., 2009. Role of suberin, suberan, and hemicellulose in phenanthrene sorption by root tissue fractions of switchgrass (*Panicum virgatum*) seedlings. Environ. Sci. Technol. 43, 4130–4136. https://doi.org/10.1021/es803510u.

Chen, L., Liu, C., Zhang, L., et al., 2017. Variation in tree species ability to capture and retain airborne fine particulate matter (PM2.5). Sci. Rep. 7, 3206. https://doi.org/10.1038/s41598-017-03360-1.

Chen, Q., Wang, F., Yang, H., Wang, X., Zhang, A., Ling, X., Li, L., Zou, P., Sun, L., Huang, L., Chen, H., Ao, L., Liu, J., Cao, J., Zhou, N., 2021. Exposure to fine particulate matter-bound polycyclic aromatic hydrocarbons, male semen quality, and reproductive hormones: The MARCHS study. Environ. Pollut. 280, 116883 https://doi.org/10.1016/j.envpol.2021.116883.

Chiam, Z., Song, X.P., Lai, H.R., Tan, H.T.W., 2019. Particulate matter mitigation via plants: understanding complex relationships with leaf traits. Sci. Total Environ. 688, 398–408. https://doi.org/10.1016/j.scitotenv.2019.06.263.

Climate Data [WWW Document], 2021. URL ⟨https://it.climate-data.org/europa/italia/campania/naples-4561/⟩.

Corada, K., Woodward, H., Alaraj, H., Collins, C.M., de Nazelle, A., 2021. A systematic review of the leaf traits considered to contribute to removal of airborne particulate matter pollution in urban areas. Environ. Pollut. Volume 269, 116104 https://doi.org/10.1016/j.envpol.2020.116104. ISSN 0269-7491.

Costabile, F., Gualtieri, M., Ancona, C., Canepari, S., Decesari, S., 2020. Ultrafine particle features associated with pro-inflammatory and oxidative responses: implications for health studies. Atmos. (Basel) 11. https://doi.org/10.3390/ATMOS11040414.

Da Luz, B.R., 2006. Attenuated total reflectance spectroscopy of plant leaves: a tool for ecological and botanical studies. New Phytol. 172 (2006), 305–318.

De Nicola, F., Maisto, G., Prati, M.V., Alfani, A., 2005. Temporal variations in PAH concentrations in *Quercus ilex* L. (holm oak) leaves in an urban area. Chemosphere 61 (3), 432–440. https://doi.org/10.1016/j.chemosphere.2005.01.082.

De Nicola, F., Lancellotti, C., Prati, M.V., Maisto, G., Alfani, A., 2011. Biomonitoring of PAHs by using *Quercus ilex* leaves: source diagnostic and toxicity assessment. Atmospheric Environment 45, 1428–1433. https://doi.org/10.1016/j.atmosenv.2010.12.022.

Deng, M., Jiang, X.L., Song, Y.G., Coombes, A., Yang, X.R., Xiong, Y.S., Li, Q.S., 2017. Leaf epidermal features of *Quercus* Group *ilex* (Fagaceae) and their application to species identification. Rev. Palaeobot. Palynol. 237, 10–36. https://doi.org/10.1016/j.revpalbo.2016.11.006.

Domínguez, E., Heredia-Guerrero, J.A., Heredia, A., 2015. Plant cutin genesis: unanswered questions. Trends Plant Sci. 20, 551–558. https://doi.org/10.1016/j.tplants.2015.05.009.

Dzierzanowski, K., Popek, R., Gawrońska, H., Saebø, A., Gawroński, S.W., 2011. Deposition of particulate matter of different size fractions on leaf surfaces and in waxes of urban forest species. Int. J. Phytoremediation 13, 1037–1046. https://doi.org/10.1080/15226514.2011.552929.

Esposito, F., Memoli, V., Panico, S.C., Di Natale, G., Trifuoggi, M., Giarra, A., Maisto, G., 2020. Leaf traits of *Quercus ilex* L. affect particulate matter accumulation. Urban For. Urban Green. 54, 126780 https://doi.org/10.1016/j.ufug.2020.126780.

Fasani, D., Fermo, P., Barroso, P.J., Martín, J., Santos, J.L., Aparicio, I., Alonso, E., 2016. Analytical method for biomonitoring of PAH using leaves of bitter orange trees (*Citrus aurantium*): a case study in South Spain. Water. Air. Soil Pollut. 227 https://doi.org/10.1007/s11270-016-3056-z.

Fellet, G., Pošćić, F., Licen, S., Marchiol, L., Musetti, R., Tolloi, A., Barbieri, P., Zerbi, G., 2016. PAHs accumulation on leaves of six evergreen urban shrubs: a field experiment. Atmos. Pollut. Res. 7, 915–924. https://doi.org/10.1016/j.apr.2016.05.007.

Fortelli, A., Scafetta, N., Mazzarella, A., 2016. Influence of synoptic and local atmospheric patterns on PM10 air pollution levels: a model application to Naples (Italy). Atmos. Environ. 143, 218–228. https://doi.org/10.1016/j.atmosenv.2016.08.050.

Fowler, D., Pilegaard, K., Sutton, M.A., Ambus, P., Raivonen, M., Duyzer, J., Simpson, D., Fagerli, H., Fuzzi, S., Schjoerring, J.K., Granier, C., Neftel, A., Isaksen, I.S.A., Laj, P., Maione, M., Monks, P.S., Burkhardt, J., Daemmgen, U., Neirynck, J., Personne, E., Wichink-Kruit, R., Butterbach-Bahl, K., Flechard, C., Tuovinen, J.P., Coyle, M., Gerosa, G., Loubet, B., Altimir, N., Gruenhage, L., Ammann, C., Cieslik, S., Paoletti, E., Mikkelsen, T.N., Ro-Poulsen, H., Cellier, P., Cape, J.N., Horváth, L., Loreto, F., Niinemets, Ü., Palmer, P.I., Rinne, J., Misztal, P., Nemitz, E., Nilsson, D., Pryor, S., Gallagher, M.W., Vesala, T., Skiba, U., Brüggemann, N., Zechmeister-Boltenstern, S., Williams, J., O'Dowd, C., Facchini, M.C., de Leeuw, G., Flossman, A., Chaumerliac, N., Erisman, J.W., 2009. Atmospheric composition change: ecosystems - atmosphere interactions. Atmos. Environ. 43, 5193–5267.

Fusaro, L., Salvatori, E., Winkler, A., Frezzini, M.A., De Santis, E., Sagnotti, L., Canepari, S., Manes, F., 2021. Urban trees for biomonitoring atmospheric particulate matter: An integrated approach combining plant functional traits, magnetic and chemical properties. Ecol. Indic. 126, 107707 https://doi.org/10.1016/j.ecolind.2021.107707.

Gong, P., Xu, H., Wang, C., Chen, Y., Guo, L., Wang, X., 2021. Persistent organic pollutant cycling in forests. Nat. Rev. Earth Environ. 2, 182–197. https://doi.org/10.1038/s43017-020-00137-5.

Grote, R., Samson, R., Alonso, R., Amorim, J.H., Cariñanos, P., Churkina, G., Fares, S., Thiec, D., Le, Niinemets, Ü., Mikkelsen, T.N., Paoletti, E., Tiwary, A., Calfapietra, C., 2016. Functional traits of urban trees: air pollution mitigation potential. Front. Ecol. Environ. 14, 543–550. https://doi.org/10.1002/fee.1426.

Heredia, A, 2003. Biophysical and biochemical characteristics of cutin, a plant barrier biopolymer. Biochimica et Biophysica Acta 1620, 1–7. https://doi.org/10.1016/s0304-4165(02)00510-x.

Heredia-Guerrero, J.A., Benítez, J.J., Domínguez, E., Bayer, I.S., Cingolani, R., Athanassiou, A., Heredia, A., 2014. Infrared and Raman spectroscopic features of plant cuticles: a review. Front. Plant Sci. 5 https://doi.org/10.3389/fpls.2014.00305.

Heredia-Guerrero, J.A., Benítez, J.J., Domínguez, E., Bayer, I.S., Cingolani, R., Athanassiou, A., Heredia, A., 2016. Infrared spectroscopy as a tool to study plant cuticles. Spectros. Eur. 28, 2.

Horemans, B., Van Holsbeke, C., Vos, W., Darchuk, L., Novakovic, V., Fontan, A.C., Backer, J., De, Van Grieken, R., De Backer, W., De Wael, K., 2012. Particle deposition in airways of chronic respiratory patients exposed to an urban aerosol. Environ. Sci. Technol. 46, 12162–12169. https://doi.org/10.1021/es302755s.

Howsam, M., Jones, K.C., Ineson, P., 2001. PAHs associated with the leaves of three deciduous tree species. II: uptake during a growing season. Chemosphere 44, 155–164. https://doi.org/10.1016/S0045-6535(00)00268-X.

Huang, W., Long, E., Wang, J., Huang, R., Ma, L., 2015. Characterizing spatial distribution and temporal variation of PM10 and PM2.5 mass concentrations in an urban area of southwest China. Atmos. Pollut. Res. 6, 842–848. https://doi.org/10.5094/APR.2015.093.

Izzo, F., Germinario, C., Grifa, C., Langella, A., Mercurio, M., 2020. External reflectance FTIR dataset (4000–400 cm^{-1}) for the identification of relevant mineralogical phases forming Cultural Heritage materials. Infrared Phys. Technol. 106, 103266 https://doi.org/10.1016/j.infrared.2020.103266.

Jouraeva, V.A., Johnson, D.L., Hassett, J.P., Nowak, D.J., 2003. Differences in accumulation of PAHs and metals on leaves of *Tilia* × *echlora* and *Pyrus calleryana*. ACS Div. Environ. Chem. - Prepr. Ext. Abstr. 43, 52–56.

Kardel, F., Wuyts, K., Babanezhad, M., Vitharana, U.W.A., Wuytack, T., Potters, G., Samson, R., 2010. Assessing urban habitat quality based on specific leaf area and stomatal characteristics of *Plantago lanceolata* L. Environ. Pollut. 158, 788–794. https://doi.org/10.1016/j.envpol.2009.10.006.

Kottek, M., Grieser, J., Beck, C., Rudolf, B., Rubel, F., 2006. World map of the Köppen-Geiger climate classification updated. Meteorol. Z. 15, 259–263. https://doi.org/10.1127/0941-2948/2006/0130.

Kováts, N., Hubai, K., Diósi, D., Sainnokhoi, T.A., Hoffer, A., Tóth, A., Teke, G., 2021. Sensitivity of typical European roadside plants to atmospheric particulate matter. Ecol. Indic. 124, 107428 https://doi.org/10.1016/j.ecolind.2021.107428.

La Riva, E.G., Villar, R., Pérez-Ramos, I.M., Quero, J.L., Matías, L., Poorter, L., Marañón, T., 2018. Relationships between leaf mass per area and nutrient concentrations in 98 Mediterranean woody species are determined by phylogeny, habitat and leaf habit. Trees 32, 497–510. https://doi.org/10.1007/s00468-017-1646-z.

Lange, O.L., Tenhunen, J.D., Braun, M., 1982. Midday stomatal closure in Mediterranean type sclerophylls under simulated habitat conditions in an environmental chamber. I. Comparison of the behaviour of various European Mediterranean species. Flora 172, 563–579.

Li, F., Gu, J., Xin, J., Schnelle-Kreis, J., Wang, Y., Liu, Z., Shen, R., Michalke, B., Abbaszade, G., Zimmermann, R., 2021. Characteristics of chemical profile, sources and PAH toxicity of PM2.5 in Beijing in autumn-winter transit season with regard to domestic heating, pollution control measures and meteorology. Chemosphere 276, 130143. https://doi.org/10.1016/j.chemosphere.2021.130143.

Li, G., Wang, L., Sun, F., Wang, Y., Wu, H., Hu, Z., Zhang, B., Yu, L., Yan, H., Shao, F., 2020. Capacity of landscaping plants to accumulate airborne particulate matter in Hangzhou, China. Polish J. Environ. Stud. 29, 153–161. https://doi.org/10.15244/pjoes/101606.

Li, Q., Li, Y., Zhu, L., Xing, B., Chen, B., 2017. Dependence of plant uptake and diffusion of polycyclic aromatic hydrocarbons on the leaf surface morphology and microstructures of cuticular waxes. Sci. Rep. 7, 1–11. https://doi.org/10.1038/srep46235.

Li, S., Tosens, T., Harley, P.C., Jiang, Y., Kanagendran, A., Grosberg, M., Jaamets, K., Niinemets, Ü., 2018. Glandular trichomes as a barrier against atmospheric oxidative stress: relationships with ozone uptake, leaf damage, and emission of LOX products across a diverse set of species. Plant Cell Environ. 41, 1263–1277. https://doi.org/10.1111/pce.13128.

Li, Y., Chen, B., Zhu, L., 2010. Single-solute and bi-solute sorption of phenanthrene and pyrene onto pine needle cuticular fractions. Environ. Pollut. 158, 2478–2484. https://doi.org/10.1016/j.envpol.2010.03.021.

Li, Y., Wang, S., Chen, Q., 2019. Potential of thirteen urban greening plants to capture particulate matter on leaf surfaces across three levels of ambient atmospheric pollution. Int. J. Environ. Res. Public Health 16. https://doi.org/10.3390/ijerph16030402.

Liu, D., Lin, T., Syed, J.H., Cheng, Z., Xu, Y., Li, K., Zhang, G., Li, J., 2017. Concentration, source identification, and exposure risk assessment of PM2.5-bound parent PAHs and nitro-PAHs in atmosphere from typical Chinese cities. Sci. Rep 7, 1–12. https://doi.org/10.1038/s41598-017-10623-4.

Liu, L., Guan, D., Peart, M.R., 2012. The morphological structure of leaves and the dust-retaining capability of afforested plants in urban Guangzhou, South China. Environ. Sci. Pollut. Res. 19, 3440–3449. https://doi.org/10.1007/s11356-012-0876-2.

Łukowski, A., Popek, R., Karolewski, P., 2020. Particulate matter on foliage of *Betula pendula*, *Quercus robur*, and *Tilia cordata*: deposition and ecophysiology. Environ. Sci. Pollut. Res. 27, 10296–10307. https://doi.org/10.1007/s11356-020-07672-0.

Mahapoonyanont, N., Mahapoonyanont, T., Pengkaew, N., Kamhangkit, R., 2010. Power of the test of one-way ANOVA after transforming with large sample size data. Procedia - Soc. Behav. Sci. 9, 933–937. https://doi.org/10.1016/j.sbspro.2010.12.262.

McPherson, E.G., Scott, K.I., Simpson, J.R., 1998. Estimating cost effectiveness of residential yard trees for improving air quality in Sacramento, California, using existing models. Atmos. Environ. 32, 75–84. https://doi.org/10.1016/S1352-2310(97)00180-5.

Mętrak, M., Aneta, E., Wiłkomirski, B., Staszewski, T., Suska-Malawska, M., 2016. Interspecific differences in foliar 1 PAHs load between Scots pine, birch, and wild rosemary from three polish peat bogs. Environ. Monit. Assess. 188, 1–13. https://doi.org/10.1007/s10661-016-5465-2.

Mo, L., Ma, Z., Xu, Y., Sun, F., Lun, X., Liu, X., Chen, J., Yu, X., 2015. Assessing the capacity of plant species to accumulate particulate matter in Beijing, China. PLoS One 10, 1–18. https://doi.org/10.1371/journal.pone.0140664.

Mori, J., Sæbø, A., Hanslin, H.M., Teani, A., Ferrini, F., Fini, A., Burchi, G., 2015. Deposition of traffic-related air pollutants on leaves of six evergreen shrub species during a Mediterranean summer season. Urban For. Urban Green. 14, 264–273. https://doi.org/10.1016/j.ufug.2015.02.008.

Niinemets, Ü., Keenan, T.F., 2014. Photosynthetic responses to stress in Mediterranean evergreens: mechanisms and models. Environ. Exp. Bot. 103, 24–41.

Niinemets, Ü., Tenhunen, J.D., Beyschlag, W., 2004. Spatial and age-dependent modifications of photosynthetic capacity in four Mediterranean oak species. Funct. Plant Biol. 31, 1179–1193.

Niinemets, Ü., Fares, S., Harley, P., Jardine, K.J., 2014. Bidirectional exchange of biogenic volatiles with vegetation: emission sources, reactions, breakdown and deposition. Plant, Cell Environ. 37, 1790–1809. https://doi.org/10.1111/pce.12322.

Nowak, D.J., Hirabayashi, S., Bodine, A., Hoehn, R., 2013. Modeled PM2.5 removal by trees in ten U.S. cities and associated health effects. Environ. Pollut. 178, 395–402. https://doi.org/10.1016/j.envpol.2013.03.050.

Orecchio, S., 2007. PAHs associated with the leaves of *Quercus ilex* L.: extraction, GC–MS analysis, distribution and sources: assessment of air quality in the Palermo (Italy) area. Atmos. Environ. 41 (38), 8669–8680. https://doi.org/10.1016/j.atmosenv.2007.07.027.

Pace, R., Grote, R., 2020. Deposition and resuspension mechanisms into and from tree canopies: a study modeling particle removal of conifers and broadleaves in different cities. Front. For. Glob. Chang. 3, 1–12. https://doi.org/10.3389/ffgc.2020.00026.

Pal, A., Kulshreshtha, K., Ahmad, K.J., Behl, H.M., 2002. Do leaf surface characters play a role in plant resistance to auto-exhaust pollution? Flora 197 (1), 47–55. https://doi.org/10.1078/0367-2530-00014.

Peng, C., Ouyang, Z., Wang, M., Chen, W., Jiao, W., 2012. Vegetative cover and PAHs accumulation in soils of urban green space. Environ. Pollut. 161, 36–42. https://doi.org/10.1016/j.envpol.2011.09.027.

Picariello, E., Baldantoni, D., Izzo, F., Langella, A., De Nicola, F., 2021. Soil organic matter stability and microbial community in relation to different plant cover: a focus on forests characterizing Mediterranean area. Appl. Soil Ecol. 162, 103897 https://doi.org/10.1016/j.apsoil.2021.103897.

Popek, R., Gawrońska, H., Wrochna, M., Gawroński, S.W., Sæbø, A., 2013. Particulate matter on foliage of 13 woody species: deposition on surfaces and phytostabilisation in waxes – a 3-year study. Int. J. Phytoremediation 15 (3), 245–256. https://doi.org/10.1080/15226514.2011.552929.

Prigioniero, A., Zuzolo, D., Niinemets, Ü., Guarino, C., 2021. Nature-based solutions as tools for air phytoremediation: a review of the current knowledge and gaps. Environ. Pollut. 277, 116817 https://doi.org/10.1016/j.envpol.2021.116817.

R Core Team, 2015. A Language and Environment for Statistical Computing. R Foundation for Statistical Computing, Vienna, Austria. -900051–07-0, URL, R.

Reich, P.B., Ellsworth, D.S., Walters, M.B., Vose, J.M., Gresham, C., Volin, J.C., Bowman, W.D., 1999. Generality of leaf trait relationships: a test across six biomes. Ecology 80, 1955–1969.

Reichstein, M., Tenhunen, J.D., Roupsard, O., Ourcival, J.-M., Rambal, S., Miglietta, F., Peressotti, A., Pecchiari, M., Tirone, G., Valentini, R., 2002. Severe drought effects on ecosystem CO_2 and H2O fluxes at three Mediterranean evergreen sites: revision of current hypothesis? Glob. Change Biol. 8, 1–19.

Riederer, M., Müller, C. (Eds.), 2006. Biology of the Cuticle. Blackwell Publishers, Oxford.

Sæbø, A., Popek, R., Nawrot, B., Hanslin, H.M., Gawronska, H., Gawronski, S.W., 2012. Plant species differences in particulate matter accumulation on leaf surfaces. Sci. Total Environ. 427–428, 347–354. https://doi.org/10.1016/j.scitotenv.2012.03.084.

Sæbø, A, Popek, R., Nawrot, B., Hanslin, H.M, Gawronska, H., Gawronski, S.W, 2012. Plant species differences in particulate matter accumulation on leaf surfaces. Science of the Total Environment 427, 347–354. https://doi.org/10.1016/j.scitotenv.2012.03.084.

Schönherr, J., 2006. Characterization of aqueous pores in plant cuticles and permeation of ionic solutes. J. Exp. Bot. 57, 2471–2491. https://doi.org/10.1093/jxb/erj217.

Sgrigna, G., Sæbø, A., Gawronski, S., Popek, R., Calfapietra, C., 2015. Particulate Matter deposition on *Quercus ilex* leaves in an industrial city of central Italy. Environ. Pollut. 197, 187–194. https://doi.org/10.1016/j.envpol.2014.11.030.

Shechter, M., Chefetz, B., 2008. Insights into the sorption properties of cutin and cutan biopolymers. Environ. Sci. Technol. 42, 1165–1171. https://doi.org/10.1021/es702205u.

Silverstein, R.M., Webster, F.X., 1998. Spectrometric Identification of Organic Compounds, sixth ed. John Wiley & Sons, New York, NY, USA, pp. 71–143.

Song, A., Liu, J., Liang, S.-G., Do, T.V., Nguyen, H.B., Deng, W.-Y.-B., Jia, L.-B., Del Rio, C., Srivastava, G., Feng, Z., Zhou, Z.-K., Huang, J., Su, T., 2021. Leaf fossils of *Sabalites* (Arecaceae) from the Oligocene of northern Vietnam and their paleoclimatic implications. Plant Divers. https://doi.org/10.1016/j.pld.2021.08.003.

Thiombane, M., Albanese, S., Di Bonito, M., Lima, A., Zuzolo, D., Rolandi, R., Qi, S., De Vivo, B., 2019. Source patterns and contamination level of polycyclic aromatic hydrocarbons (PAHs) in urban and rural areas of Southern Italian soils. Environ. Geochem. Health 41, 507–528. https://doi.org/10.1007/s10653-018-0147-3.

Tian, L., Yin, S., Ma, Y., Kang, H., Zhang, X., Tan, H., Meng, H., Liu, C., 2019. Impact factor assessment of the uptake and accumulation of polycyclic aromatic hydrocarbons by plant leaves: Morphological characteristics have the greatest impact. Sci. Total Environ. 652, 1149–1155. https://doi.org/10.1016/j.scitotenv.2018.10.357.

Tredenick, E.C., Farrell, T.W., Forster, W.A., Psaltis, S.T.P., 2017. Nonlinear porous diffusion modeling of hydrophilic Ionic agrochemicals in astomatous plant cuticle aqueous pores: a mechanistic approach. Front. Plant Sci. 8, 746. https://doi.org/10.3389/fpls.2017.00746.

Wang, H., Shi, H., 2021. Particle retention capacity, efficiency, and mechanism of selected plant species: implications for urban planting for improving urban air quality. Plants 10, 2109. https://doi.org/10.3390/plants10102109.

Wang, Q.-J., Ma, F.-J., Dong, J.-L., Yang, Y., Jin, P.-H., Sun, B.-N., 2015. Coryphoid palms from the oligocene of China and their biogeographical implications. Comptes Rendus Palevol 14 (4), 263–279. https://doi.org/10.1016/j.crpv.2015.03.005.

Wei, T., Simko, V., 2021. R package 'corrplot': Visualization of a Correlation Matrix. (Version 0.90), ⟨https://github.com/taiyun/corrplot⟩.

Wickham, H., 2016. ggplot2: Elegant Graphics for Data Analysis. Springer-Verlag, New York. ISBN 978-3-319-24277-4. https://ggplot2.tidyverse.org.

Wright, I.J., Reich, P.B., Westoby, M., Ackerly, D.D., Baruch, Z., Bongers, F., Cavender-Bares, J., Chapin, T., Cornelissen, J.H.C., Diemer, M., Flexas, J., Garnier, E., Groom, P.K., Gulias, J., Hikosaka, K., Lamont, B.B., Lee, T., Lee, W., Lusk, C., Midgley, J.J., Navas, M.L., Niinemets, Ü., Oleksyn, J., Osada, N., Poorter, H., Poot, P., Prior, L., Pyankov, V.I., Roumet, C., Thomas, S.C., Tjoelker, M.G., Veneklaas, E., Villar, R., 2004. The world-wide leaf economics spectrum. Nature 428, 821–827.

Yadav, R.K.P., Bosabalidis, A.M., Vokou, D., 2004. Leaf structural features of Mediterranean perennial species: plasticity and life form specificity. J. Biol. Res. 2, 21–34, 2004.

Zhang, L., Zhang, Z., Chen, L., McNulty, S., 2019. An investigation on the leaf accumulation-removal efficiency of atmospheric particulate matter for five urban plant species under different rainfall regimes. Atmos. Environ. 208, 123–132. https://doi.org/10.1016/j.atmosenv.2019.04.010.

Zhang, W., Wang, B., Niu, X., 2017. Relationship between leaf surface characteristics and particle capturing capacities of different tree species in Beijing. Forests 8, 1–12. https://doi.org/10.3390/f8030092.

Zhang, W., Zhang, Z., Meng, H., Zhang, T., 2018. How does leaf surface micromorphology of different trees impact their ability to capture particulate matter? Forests 9. https://doi.org/10.3390/f9110681.

Zuzolo, D., Cicchella, D., Lima, A., Guagliardi, I., Cerino, P., Pizzolante, A., Thiombane, M., Vivo, B., De, Albanese, S., 2020. Potentially toxic elements in soils of Campania region (Southern Italy): combining raw and compositional data. J. Geochem. Exp. 213, 106524 https://doi.org/10.1016/j.gexplo.2020.106524.